MAP: Low-compute Model Merging with Amortized Pareto Fronts via Quadratic Approximation

Lu Li[1*], Tianyu Zhang[2,3*], Zhiqi Bu[4*], Suyuchen Wang [5], Huan He[1], Jie Fu[6], Jiang Bian[7], Yonghui Wu[7], Yong Chen[1], Yoshua Bengio[2]

[1] University of Pennsylvania [2] MILA [3] ServiceNow [4] Amazon AGI [5] Université de Montréal
[6] HKUST [7] University of Florida
luli1@sas.upenn.edu, {Huan.He, ychen123}@pennmedicine.upenn.edu,
{tianyu.zhang, yoshua.bengio}@mila.quebec,
woodyx218@gmail.com, suyuchen.wang@umontreal.ca, fujie@ust.hk,
{bianjiang, yonghui.wu}@ufl.edu

Abstract

Model merging has emerged as an effective approach to combining multiple single-task models into a multitask model. This process typically involves computing a weighted average of the model parameters without additional training. Existing model-merging methods focus on improving average task accuracy. However, interference and conflicts between the objectives of different tasks can lead to trade-offs during the merging process. In real-world applications, a set of solutions with various trade-offs can be more informative, helping practitioners make decisions based on diverse preferences. In this paper, we introduce a novel and low-compute algorithm, **Model Merging with Amortized Pareto Front (MAP)**. MAP efficiently identifies a Pareto set of scaling coefficients for merging multiple models, reflecting the trade-offs involved. It amortizes the substantial computational cost of evaluations needed to estimate the Pareto front by using quadratic approximation surrogate models derived from a preselected set of scaling coefficients. Experimental results on vision and natural language processing tasks demonstrate that MAP can accurately identify the Pareto front, providing practitioners with flexible solutions to balance competing task objectives. We also introduce Bayesian MAP for scenarios with a relatively low number of tasks and Nested MAP for situations with a high number of tasks, further reducing the computational cost of evaluation.

1 Introduction

Large pre-trained foundation models have become widely available for many real-world applications (Wornow et al., 2023; Thirunavukarasu et al., 2023; Cui et al., 2024). This increasing availability has led to a popular practice of fine-tuning these models to adapt them to a wide range of downstream tasks. Practitioners can independently fine-tune the same pre-trained model, such as CLIP-style models (Radford et al., 2021; Wu et al., 2023; Zhai et al., 2023), large language models (Brown et al., 2020; Rozière et al., 2023; Touvron et al., 2023; Jiang et al., 2024), etc., and then release the fine-tuned models without disclosing the training data. As the deployment of such fine-tuned models increases, combining models with identical architectures and initializations has emerged as a promising approach to combine their respective capabilities. This is useful, especially in scenarios where the training data for each task is private and cannot be shared, such as individual-level patient data in hospitals and behavioral data in social media recommendation systems.

Existing methods for merging models typically involve calculating a weighted average of the parameters from multiple models to enhance performance uniformly across various tasks. However, this approach often overlooks the conflicts among the diverse objectives of these tasks, which can

[*] Equal contribution.

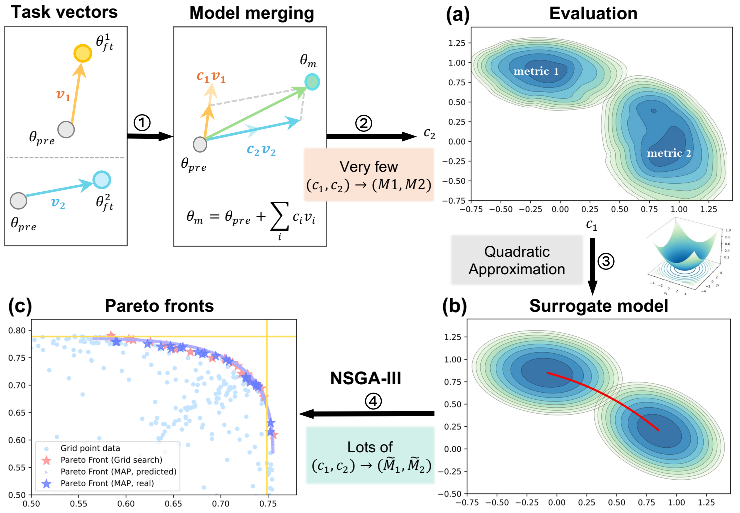

Figure 1: Illustration of the overall process of MAP for the case of two tasks. **Step 1**: Select 2 tasks and compute their corresponding task vectors. **Step 2**: Sample a few scaling coefficients **c** and query the evaluation metrics for each task, respectively. **Step 3**: Use the quadratic model as a surrogate model to approximate the mapping $\mathbf{c} \rightarrow \textit{metrics}$. **Step 4**: Use the NSGA-III algorithm with the surrogate objective functions to find amortized Pareto fronts. **(a)**: Contour plot of the actual accuracy landscape for the ViT-B/32 model (Dosovitskiy et al., 2020) obtained from 100 scaling coefficients (sampled uniformly) evaluated on the SUN397 (Xiao et al., 2016) and Cars (Krause et al., 2013) datasets. **(b)**: Contour plot of the fitted quadratic functions. Red lines represent the Pareto front in the decision variable (c_1, c_2) space. **(c)**: Example of the resulting Pareto fronts. The Pareto front (Grid search) is regarded as the ground truth given the sufficient number of grid points evaluated. The Pareto front (MAP, predicted) is the amortized Pareto front. The Pareto front (MAP, real) corresponds to the same $\{(c_1, c_2)\}$ but is re-evaluated to obtain the ground truth metrics for comparison. The yellow lines indicate the evaluated performance of the fine-tuned single-task models.

lead to trade-offs in model performance across different tasks. In real-world applications, it is often more beneficial to obtain a set of Pareto optimal solutions rather than a single model. Such solutions allow practitioners to choose among different trade-offs based on their specific needs. For example, hospitals specializing in certain areas might prefer a model that excels in tasks relevant to their specialty while maintaining adequate performance across a broader spectrum of diseases.

In this paper, we introduce a novel method that identifies the Pareto front without retraining the models to be merged. Our algorithm utilizes a quadratic approximation of the evaluation metric. Furthermore, we enhance it with a Bayesian adaptive sampling method and a nested merging scheme, which further reduces the computational cost. We validate our method across a diverse set of tasks, spanning from vision to natural language processing, and demonstrate its applicability to a variety of architectures, including ResNets (He et al., 2016), ViT (Dosovitskiy et al., 2020), and large language models (Brown et al., 2020; Rozière et al., 2023; Touvron et al., 2023; Jiang et al., 2024). Our results confirm that this novel approach supports the seamless integration of diverse model capabilities and aligns more closely with various real-world preferences by providing a set of optimal fronts across the tasks.

Contributions The main contributions of this paper are:

C1 We propose the MAP algorithm, which utilizes quadratic surrogate models to approximate evaluation metric functions, thereby amortizing the computation of Pareto fronts.

C2 We demonstrate the effectiveness of MAP across a diverse set of architectures, including vision models (e.g., ResNet, ViT) and large language models, highlighting its generalizability and flexibility across different domains.

C3 We introduce two variants of MAP: the nested-merging MAP, which reduces computational complexity from $O(N \cdot 2^N)$ to $O(N \log N)$, and the Bayesian MAP, which efficiently queries computationally expensive evaluations based on loss information.

C4 To the best of our knowledge, this paper is the first work to estimates the Pareto front for task-vector-based model-merging methods with low compute, and without relying on gradient descent for deep neural networks. Our code is available at `https://github.com/luli-git/MAP`.

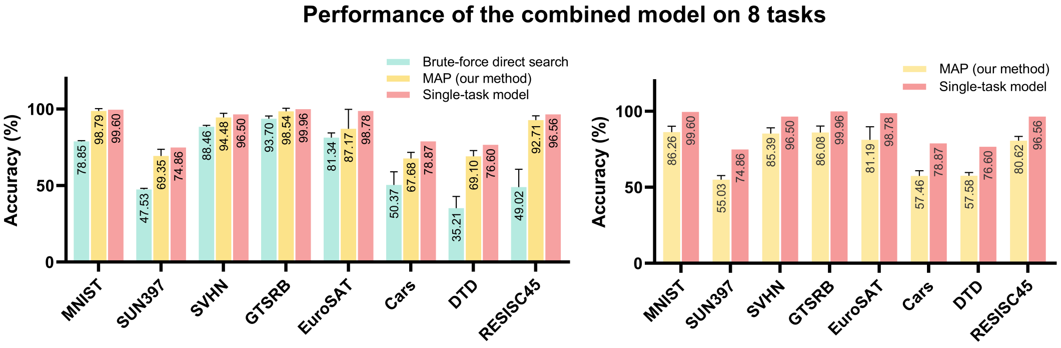

Figure 2: **Left**: Comparison of our method with direct search for merged ViT-B/32 models (Dosovitskiy et al., 2020), based on evaluation results of 250 combinations of scaling coefficients. Our method identifies a more diverse set of solutions across eight tasks within the same computational budget. Both methods aim to maximize the performance of one task while ensuring that all other tasks meet a minimum threshold of 40%. The bar plot displays the maximized accuracy for each task. **Right**: When the threshold is increased to 65% of the single-task model's performance, the brute-force direct search method fails to find any feasible solutions within the same computational budget.

In Figure 2, we compare our method to direct search. It is important to note that evaluating models in our problem setting is computationally expensive; as a result, our proposed method can only query the evaluation pipeline a limited number of times. We choose to compare with direct brute-force search within the scaling coefficient spaces. When the number of tasks is low, the Pareto fronts obtained through direct brute-force search can be considered ground truth because the scaling coefficient spaces have been sufficiently explored. However, when the number of tasks is high, we may not be able to derive reasonable ground truth Pareto fronts using direct brute-force search. Nonetheless, we can still demonstrate the efficiency of our method by comparing the winning ratio of MAP to that of direct brute-force search.

2 Background

2.1 Model merging

Model merging aims to combine two or more trained models into a single model to leverage the strengths of each and improve overall performance (Deep et al., 2024; Shoemake, 1985; Wang et al., 2024b). A recent work by Ilharco et al. (2022) introduced *task arithmetic* as a simple and effective method for model merging. The task vector for task n is defined as $\mathbf{v}_n = \boldsymbol{\theta}_{ft}^n - \boldsymbol{\theta}_{\text{pre}}$, which is the element-wise difference between the pre-trained weights and the fine-tuned weights for task n. To perform model merging with task vectors, we can compute the merged model as $\boldsymbol{\theta}_m = \boldsymbol{\theta}_{\text{pre}} + \sum_{n=1}^{N} c_n \mathbf{v}_n$, where c_n are the scaling coefficients that have been shown to be essential for the performance of the merged model (Yadav et al., 2024; Yang et al., 2023).

Denoting the metric of task n as M_n, most existing approaches to model merging aim to improve an equal weight average metric $\frac{1}{N}\sum_{n=1}^{N} M_n$. This target implies that the user of the algorithm has no preferences between tasks. However, in real-world applications, users may have biased preferences for the importance of tasks, necessitating trade-offs in model performance. In such cases, the goal of model merging shifts from the simple average metric to addressing a broader question:

Given any preferences over the set of tasks, what is the best way to merge the models?

2.2 Pareto fronts

Definition 1 (Pareto dominance)**.** *Let X be a set representing the solution space, where each element $x \in X$ is a possible solution to the multi-objective optimization problem. Let there be n objectives, and define an evaluation loss function $f_i : X \to \mathbb{R}$, where $i \in \{1, 2, \ldots, n\}$.*

Given two solutions $x, y \in X$, we define that x Pareto dominates y, denoted by $x \succ_P y$, if and only if:

$$\forall i \in \{1, 2, \ldots, n\}, f_i(x) \leq f_i(y) \textit{ and } \exists j \in \{1, 2, \ldots, n\}, f_j(x) < f_j(y)$$

Definition 2 (Pareto optimal solutions)**.** *The Pareto front is the set of solutions in the solution space X that are not Pareto dominated by any other solutions in X. The Pareto front is given by:*

$$PF = \{x \in X \mid \nexists y \in X \textit{ s.t. } y \succ_P x\} \tag{1}$$

Pareto optimal solutions have been studied in multi-task (multi-objective) learning (MTL) (Sener & Koltun, 2018; Lin et al., 2019). However, in most of the studies, approximating the Pareto front is computationally expensive and data inefficient. We introduce our method, MAP, a computationally efficient method to find the Pareto front for model merging.

3 Methods

In this section, we discuss the proposed MAP method in detail. To enhance readability, we present a table of notations in Table 5.

3.1 Quadratic approximation of evaluation metric

Given the task vectors $\{\mathbf{v}_n\}_{\{n=1,\ldots,N\}}$ and the initialization $\boldsymbol{\theta}_{\text{pre}} \in \mathbb{R}^d$, we denote the merged model parameters as $\boldsymbol{\theta}_m(\mathbf{c}) = \boldsymbol{\theta}_{\text{pre}} + \mathbf{V}\mathbf{c} = \boldsymbol{\theta}_{\text{pre}} + \sum_{n=1}^{N} c_n \mathbf{v}_n$, where $\mathbf{V} = \text{concat}(\mathbf{v}_1, ..., \mathbf{v}_N) \in \mathbb{R}^{d \times N}$ is the task matrix and $\mathbf{c} = [c_1, ..., c_N]^\top \in \mathbb{R}^N$ is the vector of scaling coefficients for the task vectors.

Let $M_n(\mathbf{c}) = M_n(\theta_m(\mathbf{c}))$ denote the evaluation metric for task n of the merged model. We aim to optimize the evaluation metric for each task via the multi-objective optimization problem (MOOP)[1]:

$$\min_{c_1,\ldots,c_N} M_1(\mathbf{c}), \ldots, M_N(\mathbf{c}) \tag{2}$$

This problem has N variables and N objectives, and we seek the Pareto optimal solutions.

Motivated by the observation that the finetuned models tend to have parameters close to the pretrained model (as shown in Table 1), we present the following assumption.

Assumption 1. *The task vectors $\mathbf{v}_n$ have small norms relative to the pretrained model parameters $\boldsymbol{\theta}_{\text{pre}}$, i.e., $|\mathbf{v}_n| \ll |\boldsymbol{\theta}_{\text{pre}}|$ for $n = 1, \ldots, N$. Additionally, the evaluation metrics $M_n(\theta)$ are sufficiently smooth around $\boldsymbol{\theta}_{\text{pre}}$, such that higher-order terms in their Taylor expansions are negligible within the region defined by the task vectors.*

Denote p as the number of parameters in the pre-trained model and also as the number of parameters in each task vector. Let N represent the number of tasks.

To derive our algorithm, MAP, we utilize the second-order Taylor expansion to approximate M_n:

$$\begin{aligned} M_n(\mathbf{c}) \equiv M_n(\boldsymbol{\theta}_{\text{m}}(\mathbf{c})) &= M_n(\boldsymbol{\theta}_{\text{pre}}) + \nabla M_n(\boldsymbol{\theta}_{\text{pre}})^\top (\boldsymbol{\theta}_m(\mathbf{c}) - \boldsymbol{\theta}_{\text{pre}}) \\ &\quad + \frac{1}{2}(\boldsymbol{\theta}_m(\mathbf{c}) - \boldsymbol{\theta}_{\text{pre}})^\top \mathbf{H}_n(\boldsymbol{\theta}_{\text{pre}})(\boldsymbol{\theta}_m(\mathbf{c}) - \boldsymbol{\theta}_{\text{pre}}) + R_n(\boldsymbol{\theta}_m(\mathbf{c}) - \boldsymbol{\theta}_{\text{pre}}) \\ &= \underbrace{M_n(\boldsymbol{\theta}_{\text{pre}})}_{\in\mathbb{R}} + \underbrace{\nabla M_n(\boldsymbol{\theta}_{\text{pre}})^\top}_{\in\mathbb{R}^{1\times p}} \underbrace{\mathbf{V}}_{\in\mathbb{R}^{p\times N}} \underbrace{\mathbf{c}}_{\in\mathbb{R}^{N\times 1}} + \frac{1}{2} \underbrace{(\mathbf{V}\mathbf{c})^\top}_{\in\mathbb{R}^{1\times p}} \underbrace{\mathbf{H}_n(\boldsymbol{\theta}_{\text{pre}})}_{\in\mathbb{R}^{p\times p}} \underbrace{\mathbf{V}\mathbf{c}}_{\in\mathbb{R}^{p\times 1}} + \underbrace{R_n}_{\in\mathbb{R}} \end{aligned}$$

where $\mathbf{H}_n(\boldsymbol{\theta}_{\text{pre}}) = \nabla^2 M_n(\boldsymbol{\theta}_{\text{pre}}) \in \mathbb{R}^{d\times d}$ is the Hessian matrix and $R_n(\boldsymbol{\theta}_m(\mathbf{c}) - \boldsymbol{\theta}_{\text{pre}}) = R_n(\mathbf{V}\mathbf{c})$ is the third-order remainder, which, as stated in Assumption 1, is negligible when $||\mathbf{V}\mathbf{c}||^3 = ||\boldsymbol{\theta}_m(\mathbf{c}) -$

[1] The evaluation metric M can be differentiable (e.g., mean square loss or cross-entropy/perplexity) or not necessarily (e.g., classification accuracy, F1 score, BLEU, or Rouge)

$\boldsymbol{\theta}_{\text{pre}}||^3$ is small. Note that the second-order Taylor expansion is widely used (McCandlish et al., 2018; Bu et al., 2024; Kaplan et al., 2020; Hoffmann et al., 2022) and provides a close approximation (see Figure 2 (a) and (b) and more discussion in Appendix 5).

Table 1: We compute the L_1 norm of the weight matrices of the pretrained models and the task vectors for each of the 8 tasks using the ViT-B/32 model, and compute the ratio.

Metric	SUN397	Cars	DTD	SVHN	RESISC45	MNIST	GTSRB	EuroSAT
$\|\|\boldsymbol{\theta}_{pre}\|\|_1$	1,270,487	1,270,487	1,270,487	1,270,487	1,270,487	1,270,487	1,270,487	1,270,487
$\|\|\mathbf{v}_n\|\|_1$	21,055	20,127	13,621	19,349	18,409	17,578	16,712	15,941
$\|\|\mathbf{v}_n\|\|_1/\|\|\boldsymbol{\theta}_{pre}\|\|_1(\%)$	1.66%	1.58%	1.07%	1.52%	1.45%	1.38%	1.32%	1.25%

To validate the approximation, we calculate the L_1 norm of the parameters for the 8 task vectors and their ratios relative to the L_1 norm of the pretrained model. As shown in Table 1, the ratio between the L_1 norm of the task vectors and the L_1 norm of the weight matrices of the pretrained model is approximately 1% to 2% for each of the 8 tasks.

We further examine the density plot of the absolute values of the weight matrices of the 8 task vectors (Figure 3). We find that the maximum magnitude of the task vectors is 0.00859, while the mean is 1.57336 $\times 10^{-4}$. These findings motivate and validate our key assumption 1 of using a second-order Taylor expansion to approximate the evaluation metrics.

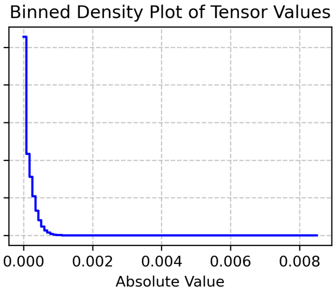

Figure 3: Density plot of the absolute values of the weight matrices of the 8 task vectors.

Leveraging this quadratic approximation, we can define surrogate models for each task N,

$$\tilde{M}_n(\mathbf{c}; \mathbf{A}_n, \mathbf{b}_n, e_n) \equiv \frac{1}{2}\mathbf{c}^\top \mathbf{A}_n \mathbf{c} + \mathbf{b}_n^\top \mathbf{c} + e_n \tag{3}$$

and optimize the proxy problem of Equation (2) via

$$\min_{c_1,\ldots,c_N} \tilde{M}_1(\mathbf{c}), \ldots, \tilde{M}_N(\mathbf{c}) \tag{4}$$

where $\mathbf{A}_n \in \mathbb{R}^{N\times N}$ is parameter matrix approximating $\mathbf{V}^\top \mathbf{H}_n(\boldsymbol{\theta}_{\text{pre}})\mathbf{V}$; $\mathbf{b}_n \in \mathbb{R}^N$ is a parameterized vector targeting to $\mathbf{V}^\top \nabla M_n(\boldsymbol{\theta}_{\text{pre}})$; e_n is a parameter scalar which estimates $M_n(\boldsymbol{\theta}_{\text{pre}}) + R_n$.

Importantly, Equation (4) is parameterized in contrast to Equation (2), with a total of $\frac{(N+1)(N+2)}{2}$ surrogate model parameters in (e_n, $\mathbf{b}_n$, $\mathbf{A}_n$), i.e., 1 coefficient for e_n, N coefficients in $\mathbf{b}_n$ and $N(N+1)/2$ coefficients in $\mathbf{A}_n$ due to its symmetry ($1 + N + \frac{N(N+1)}{2} = \frac{(N+1)(N+2)}{2}$). We do not calculate the gradient or Hessian to obtain the parameters $\mathbf{A}_n$, $\mathbf{b}_n$, e_n. Instead, we estimate them by minimizing the MSE between M_n and $\tilde{M}_n$, $n = 1, \ldots, N$:

$$\mathbf{A}_n^*, \mathbf{b}_n^*, e_n^* = \arg\min_{\mathbf{A}_n, \mathbf{b}_n, e_n} \sum_{\mathbf{c}\in\Omega} |M_n(\boldsymbol{\theta}_{\text{merge}}(\mathbf{c})) - \tilde{M}_n(\mathbf{c}; \mathbf{A}_n, \mathbf{b}_n, e_n)|^2 \tag{5}$$

where $\Omega = \{\mathbf{c}^{(1)}, \ldots, \mathbf{c}^{(K)}\}$ is the set of $\mathbf{c}$ and $M_n(\boldsymbol{\theta}_{\text{merge}}(\mathbf{c}))$ is the corresponding evaluation metric. Below we discuss 3 extensive cases of this problem.

Case 1: If the evaluation metric spans the whole real-number axis $\mathbb{R}$, we use the vanilla form of the surrogate model in Equation (3). As shown in Corollary 1, we have a closed-form solution for Equation (5)

Corollary 1 (Closed-form Solution for Surrogate Model Parameters)**.** *Under Assumption 1, for each task $n = 1, \ldots, N$, the optimization problem 5 is equivalent to solving a linear regression where the predictors include all quadratic, interaction, linear, and constant terms of $\mathbf{c}$. The closed-form solution for the parameters is given by*

$$\begin{pmatrix} vec(A_n^*) \\ \mathbf{b}_n^* \\ e_n^* \end{pmatrix} = \left(\mathbf{C}_n^\top \mathbf{C}_n\right)^{-1} \mathbf{C}_n^\top \mathbf{y}_n$$

where $\mathbf{C}_n(\mathbf{c}) = (c_1^2, c_2^2, \dots, c_N^2, c_1c_2, c_1c_3, \dots, c_{N-1}c_N, c_1, c_2, \dots, c_N, 1)$*, and* $\mathbf{y}_n$ *is the vector of observed metrics* $M_n(\theta_m(\mathbf{c}))$ *for all* $\mathbf{c} \in \Omega$*. Please refer to Corollary 3 for a more detailed corollary.*

Case 2: When the evaluation metric is restricted to a specific range $[l, u]$, e.g. accuracy is restricted to $[0, 1]$, we can apply a sigmoid transformation to the quadratic term, i.e.

$$\tilde{M}_n(\mathbf{c}; \mathbf{A}_n, \mathbf{b}_n, e_n) \equiv (u - l)\sigma(e_n + \mathbf{b}_n^\top \mathbf{c} + \frac{1}{2}\mathbf{c}^\top \mathbf{A}_n \mathbf{c}) + l.$$

Case 3: Similarly, when the evaluation metric is restricted to $[l, +\infty)$, applying a softplus transformation ensures non-negativity while allowing smooth growth. In this case, we define:

$$\tilde{M}_n(\mathbf{c}; \mathbf{A}_n, \mathbf{b}_n, e_n) \equiv \text{softplus}(e_n + \mathbf{b}_n^\top \mathbf{c} + \frac{1}{2}\mathbf{c}^\top \mathbf{A}_n \mathbf{c}) + l,$$

where $\text{softplus}(x) = \ln(1 + e^x)$.

In Cases 2 and 3, the parameters u and l are not learnable parameters but predefined based on the feasible range of the metric. The introduction of non-linear functions in $\tilde{M}_n$ eliminates closed-form solutions, necessitating the use of gradient descent to solve the optimization problem 5. Despite this, the approach remains computationally efficient since the number of parameters in the surrogate model is $\frac{(N+1)(N+2)}{2}$. We emphasize that gradient descent on the surrogate model is computationally efficient. Compared to training full-scale deep learning models, this method requires significantly fewer computations. For instance, when merging eight models, the parameter count is only 45, which is much smaller than the millions of parameters typically found in deep learning architectures.

3.2 Model merging with amortized Pareto fronts

In this section, we introduce our generalized algorithm for estimating the amortized Pareto fronts. As mentioned in Section 3.1, we approximate the evaluation metric $M_n(\cdot)$ by a surrogate quadratic model $\tilde{M}_n(\cdot)$. We then utilize $\tilde{M}_n(\cdot)$ to compute the amortized Pareto fronts. Please see the detailed experiments in Section 4 and the algorithm details in Algorithm 1. Different from other Pareto multi-task learning algorithms, our algorithm does not require calculating the gradients or performing gradient descent on the deep learning model parameters.

Algorithm 1 MAP

```
Input: Pretrained model $\boldsymbol{\theta}_{pre}$, fine-tuned models $\{\boldsymbol{\theta}_{ft}^n\}_{n=1}^N$.
Compute task vectors $\{\mathbf{v}_n = \boldsymbol{\theta}_{ft}^n - \boldsymbol{\theta}_{\text{pre}} \mid n \in 1, \dots, N\}$.
Sample $K$ vectors of $\mathbf{c} \in \mathbb{R}^N$. Denote the set as $\Omega$.
for $n \in [N]$ do
    for $\mathbf{c} = [c_1, ..., c_N] \in \Omega$ do
        Compute $\boldsymbol{\theta}(\mathbf{c}) = \boldsymbol{\theta}_{\text{pre}} + c_1\mathbf{v}_1 + \ldots + c_N\mathbf{v}_N$.
        Obtain the evaluation metric $M_n(\boldsymbol{\theta}(\mathbf{c}))$.
    end
    Fit the quadratic approximation surrogate model $\tilde{M}_n$ by learning $\mathbf{A}_n^*, \mathbf{b}_n^*, e_n^*$ in Equation (5).
end
Apply MOOP algorithm (e.g. NSGA-III) to $\{\tilde{M}_n\}$ and find the Pareto front
```

3.3 Further methods to bring down the computation cost when the number of tasks is high

In addition to MAP, we also introduce nested merging MAP (NMMAP) and Bayesian MAP (BMAP), which are variants of MAP designed to further reduce computation costs.

For a small number of tasks ($N \leq 3$), we use Bayesian adaptive sampling, inspired by Bayesian optimization. Unlike plain MAP (Algorithm 1), which samples a single set of scaling weights $\mathbf{c}$ and evaluates metrics $M_n(\boldsymbol{\theta}(\mathbf{c}))$, Bayesian adaptive sampling iteratively samples $\mathbf{c}$ across multiple rounds, with each round informed by prior evaluations.

The process starts with uniform sampling of scaling coefficients $\{(c_1, \dots, c_N)\}$, from $[0, 1]^N$, evaluating the merged models $\theta_m(\mathbf{c}_i)$ for tasks 1 to N, and calculating the L_2 loss. We compute a posterior distribution based on an acquisition function, like the upper confidence bound, for each bin.

We iteratively update surrogate models for each task, and after meeting the stopping criterion, generate $(\mathbf{c}, \{\tilde{M}_n(\theta_m(\mathbf{c}))\}_{n=1}^N)$ samples. A MOOP algorithm (e.g., NSGA-III) is then applied to compute the Pareto front from $\tilde{M}_n$.

As illustrated in Figure 4 (a), BMAP uses Bayesian optimization to determine the distribution of scaling coefficients for task vectors when approximating the surrogate model in MAP. For more details and experiments, please refer to Appendix E.3.

When the number of tasks N is high and computational resources are also limited, NMMAP reduces the number of evaluations from $O(TN2^N)$ to $O(N \log N)$. For example, tasks 1 to 8 cover Cars, GTSRB, DTD, SUN397, RESISC45, MNIST, EuroSAT, and SVHN. With nested merging, in the first round, we merge $(\boldsymbol{\theta}_{ft}^1, \boldsymbol{\theta}_{ft}^2)$ into $\boldsymbol{\theta}_{\text{merge}}^{1,2}$. Similarly, we merge $(\boldsymbol{\theta}_{ft}^3, \boldsymbol{\theta}_{ft}^4)$into $\boldsymbol{\theta}_{\text{merge}}^{3,4}$, $(\boldsymbol{\theta}_{ft}^5, \boldsymbol{\theta}_{ft}^6)$ into $\boldsymbol{\theta}_{\text{merge}}^{5,6}$ and $(\boldsymbol{\theta}_{ft}^7, \boldsymbol{\theta}_{ft}^8)$ into $\boldsymbol{\theta}_{\text{merge}}^{7,8}$ in parallel. Next, we merge $(\boldsymbol{\theta}_{\text{merge}}^{1,2}, \boldsymbol{\theta}_{\text{merge}}^{3,4})$ into $\boldsymbol{\theta}_{\text{merge}}^{1,2,3,4}$, and $(\boldsymbol{\theta}_{\text{merge}}^{5,6}, \boldsymbol{\theta}_{\text{merge}}^{7,8})$ into $\boldsymbol{\theta}_{\text{merge}}^{5,6,7,8}$ simultaneously and finally into $\boldsymbol{\theta}_{\text{merge}}^{1,2,3,4,5,6,7,8}$. Note that the model merging order is illustrative and chosen to support the exposition.

This approach achieves a 250x speedup when the number of tasks is 8, while also outperforming direct search methods. However, it can no longer output the complete Pareto front for all tasks, and practitioners need to be able to quantify their preferences during the merging since it merges models in pairs in a nested fashion, as shown in Figure 4 (b). For more details and experiments, please refer to Appendix E.2.

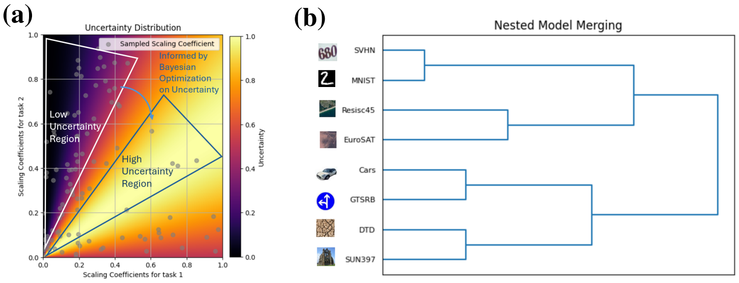

Figure 4: **(a)**: Utilize Bayesian optimization to guide the sampling of scaling coefficients according to the uncertainty distribution; **(b)**: An example of nested model merging for $N = 8$ models.

4 Experiments

Datasets and models We evaluate multi-task model merging on eight zero-shot image classification datasets following (Ilharco et al., 2022): SUN397 (Xiao et al., 2016), Cars (Krause et al., 2013), GTSRB (Stallkamp et al., 2011), MNIST (LeCun, 1998), EuroSAT (Helber et al., 2019), SVHN (Netzer et al., 2011), DTD (Cimpoi et al., 2014), and RESISC45 (Cheng et al., 2017). We use the ViT-B/32 architecture in CLIP (Radford et al., 2021) as the pre-trained model for the experiments on vision tasks discussed in the main text. We show the results of these experiments in the main pages.

The rest of the experiments are presented in the Appendix due to page limits. The results from the datasets and tasks we experimented on are as follows: a zero-shot medical chest X-ray image classification task to show our model merging scheme works in a real-world application in the medical domain (Wang et al., 2017) (Appendix D.3); four fine-tuned Llama3 models in different languages: French, Arabic, Chinese, and Japanese (Appendix D.4)[2]; and three vision classification tasks using the ResNet18 (He et al., 2016) architecture: CIFAR-10 (Krizhevsky et al., 2009), Flowers-102 (Nilsback & Zisserman, 2008), and GTSRB (Stallkamp et al., 2011) to show that our model merging scheme also works with other model architectures (Appendix D.5).

[2] All the fine-tuned language Llama3 models can be found on Hugging Face. The IDs of the models are: French: jpacifico/French-Alpaca-Llama3-8B-Instruct-v1.0; Arabic: MohamedRashad/Arabic-Orpo-Llama-3-8B-Instruct; Chinese: shenzhi-wang/Llama3-8B-Chinese-Chat; Japanese: haqishen/Llama-3-8B-Japanese-Instruct.

4.1 Baseline and metrics

Pareto front-finding baselines One of our baseline methods for obtaining Pareto fronts is the brute-force direct search, which can be regarded as the gold standard when the number of tasks is low ($N < 4$). This is because we can sample enough grid points of $\mathbf{c}$ and query the corresponding evaluation metrics $\{M_n(\theta(\mathbf{c}))\}_{n=1}^N$. We can then directly use the resulting evaluation metrics to find the Pareto front by direct comparisons of each task's performance of the merged model by $c_i \in \mathbf{c}$.

Another baseline method for finding Pareto fronts is the Multi-Objective Evolutionary Algorithm based on Decomposition (MOEA/D) (Zhang & Li, 2007). Key hyperparameters in MOEA/D include the population size and the number of generations, which significantly influence its performance by affecting the quality and diversity of the resulting Pareto front as well as the computational cost.

It is important to note that when the number of tasks grows, the required number of $(\mathbf{c}, \{M_n(\theta(\mathbf{c}))\}_{n=1}^N)$ pairs grows exponentially for the brute force method, as well as for the MOEA/D method, which is much larger than the points we can evaluate given the computational constraint. Thus, when the number of tasks is high ($N \geq 4$), the results from the brute-force direct search can no longer be considered ground truth. In Appendix E.2.2, we show an illustration of why the curse of dimensionality occurs when the number of tasks increases.

Single merged model baselines In addition to the brute-force method and MOEA/D, we compare with other model merging methods including SLERP (Shoemake, 1985), TIES-merging (Yadav et al., 2024), Task Arithmetic with a single scalar (Ilharco et al., 2022), Task Arithmetic with preferences as scalars (Ilharco et al., 2022), DARE combined with Task Arithmetic (Yu et al., 2023; Ilharco et al., 2022), and DARE combined with TIES-merging (Yu et al., 2023; Yadav et al., 2024).

Win rate We used the win rate to measure how often the Pareto front found by MAP outperforms the Pareto front found by the baseline in terms of multiple objectives. Let PF_{MAP} and $PF_{baseline}$ represent the set of solutions in the Pareto fronts obtained from the MAP and the baseline methods, respectively. Each solution in these sets is a vector in $\mathbb{R}^N$, where N is the number of objectives or tasks. We sampled $K = 100$ points from the decision space of each of the two Pareto fronts, denoted as $\mathbf{c}_k^{MAP}$ and $\mathbf{c}_k^{baseline}, k = 1, \ldots, K$. Then, we compared $M_n(\theta(\mathbf{c}_k^{MAP}))$ and $M_n(\theta(\mathbf{c}_k^{baseline}))$ pairwise for $k = 1, \ldots, K$ and $n = 1, \ldots, N$, resulting in K^2N comparisons. The ratio of instances where $M_n(\theta(\mathbf{c}_k^{MAP})) > M_n(\theta(\mathbf{c}_k^{baseline}))$ is computed as the win rate of PF_{MAP}:

$$\text{Win Rate} = \frac{1}{K^2N} \sum_{i=1}^{K} \sum_{j=1}^{K} \sum_{n=1}^{N} \mathbb{I}\left[M_n(\theta(\mathbf{c}_i^{\text{MAP}})) > M_n(\theta(\mathbf{c}_j^{\text{baseline}}))\right]$$

where $K = 100$, $\mathbf{c}_i^{\text{MAP}} \in$ Decision Space of $PF_{\text{MAP}}, i = 1, \ldots, K$, $\mathbf{c}_j^{\text{baseline}} \in$ Decision Space of $PF_{\text{baseline}}, j = 1, \ldots, K, \mathbb{I}[\cdot]$ is the indicator function.

4.2 Win rate of MAP over the direct search method

Table 2 shows the results for the win rate of MAP over the brute force direct search method **when the number of tasks is small (**$N < 4$**)**. In such cases, the Pareto front can be regarded as the ground truth Pareto front, and we can only query 30 and 50 scaling coefficients to achieve similar performance with the ground truth Pareto front.

Table 3 shows the results for the win rate of MAP over the brute force direct search method **when the number of tasks is high (**$N \geq 4$**)**. The Pareto front generated by the brute force method can no longer be considered ground truth due to the limited number of points per dimension that is covered. In this setting, MAP performs much better than the brute-force (not ground truth) Pareto solutions.

Table 2: Win rate of the amortized PF over the brute-force direct search PF, where the latter can be regarded as the ground truth when $N < 4$. # **c** is the number of scaling coefficient vectors each algorithm evaluated to find the Pareto front. # **c** per dim = (# **c** direct search)$^{1/N}$ measures the sparsity of points the direct search method uses, as illustrated in Figure 11.

N	# **c** (direct search)	# **c** per dim	# **c** (MAP)	Win rate (MAP)	R^2 (MAP)
2	200	14.14	30	49.81% (±0.30)	0.953 (±0.018)
3	300	6.69	50	46.90% (±0.71)	0.980 (±0.003)

Table 3: Win rate of the amortized PF over the brute-force direct search PF, where the latter can **no longer** be regarded as the ground truth when $N \geq 4$. # of $\mathbf{c}$ is the number of scaling coefficient vectors each algorithm evaluated to find the Pareto front. # $\mathbf{c}$ per dim = (# $\mathbf{c}$ direct search)$^{1/N}$ measures the sparsity of points the direct search method uses, as illustrated in Figure 11.

N	# $\mathbf{c}$ (direct search)	# $\mathbf{c}$ per dim	# $\mathbf{c}$ (MAP)	Win rate (MAP)	R^2 (MAP)
4	300	4.16	60	50.67% (±2.44)	0.984 (±0.004)
5	500	3.47	85	53.00% (±1.88)	0.941 (±0.019)
6	500	2.82	100	60.71% (±1.34)	0.941 (±0.030)
7	1000	2.68	140	63.42% (±1.91)	0.891 (±0.024)
8	1000	2.37	250	65.58% (±0.94)	0.868 (±0.028)

4.3 Comparing with other single merged model baseline methods

We compared the performance of MAP with TIES-merging (Yadav et al., 2023), TIES-merging with DARE (Yu et al., 2023), Task Arithmetic with DARE, Task Arithmetic with normalized preference as scaling coefficients (Ilharco et al., 2023), Ada-merging++ (Yang et al., 2024), DELLA-merging (Deep et al., 2024) and SLERP (Shoemake, 1985). For dimension 2, we can directly visualize the results, as shown in Figure 5. The solutions found by MOEA/D exhibited clustering and a lack of adequate spread across the Pareto front. In addition, the computational cost of MOEA/D was significantly higher than that of MAP. For example, with a population size of 50 and 20 generations (which produced the best results for MOEA/D in terms of diversity as shown in Figure 5), the total number of evaluations amounted to 2500 for two tasks. In comparison, MAP achieved its results with only 60 total evaluations—a reduction of over 95%. This highlights the computational efficiency of MAP in obtaining a diverse and high-quality Pareto front.

MAP offers a well-distributed set of Pareto optimal solutions None of the baseline methods can directly dominate all Pareto solutions found by MAP, and most of them lie either within or on the Pareto front found by MAP. In addition, we sampled 10 points from the predicted Pareto front generated by MAP and evaluated them (MAP Pareto solutions, real) to confirm that they indeed lie close to the predicted Pareto front. This evidence further confirms the usefulness of MAP as a general strategy for finding a diverse and well-distributed set of Pareto solutions that none of the existing model merging methods can substitute.

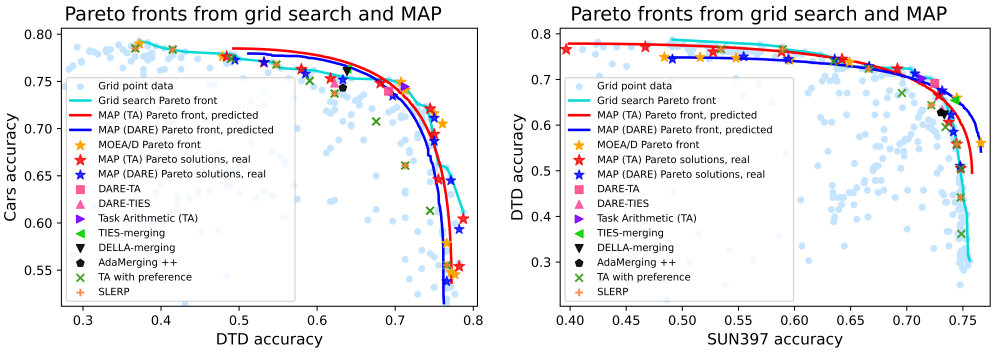

Figure 5: The Pareto fronts obtained using MAP with Task Arithmetic, MAP with Task Arithmetic and DARE. We sampled 10 Pareto solutions from the predicted front by MAP and evaluated them to obtain the real values. We plotted the results obtained using TIES-merging, Task Arithmetic (TA) with a single scalar for all tasks, Task Arithmetic with preferences as scalars, TA combined with DARE (DARE-TA), TIES-merging combined with DARE (DARE-TIES), and SLERP.

MAP is an out-of-the-box plugin for other task-vector based model merging methods As shown in Figure 5, MAP is a plug-in that can be directly combined with other model merging methods, allowing users to control their preferences over each task using scaling coefficients. For example, MAP can be combined with DARE, Task Arithmetic, etc.

For dimensions higher than 2, we use preference-weighted evaluation sum to compare the Pareto front found by MAP with other baseline methods. We sample 20 preference vectors and normalize them. Then, we pick the solution by MAP that maximizes the preference-weighted sum of accuracies and compare it with those of the baseline methods. The results are shown in Table 4. We observe that even in higher dimensions, when users have specific preferences, MAP remains effective and can better accommodate those preferences. Note that when using MAP, users are not required to pre-specify their preference vector. In fact, users can obtain the entire Pareto front to better understand the trade-offs. This preference vector-based metric is solely for evaluation.

Table 4: We compared MAP with a set of baseline methods by sampling a set of 20 normalized preference vectors and computing the preference-weighted sum of accuracies. $\uparrow$ indicates higher is better. The number after $\pm$ is the standard deviation. Please refer to Table 2 and Table 3 for the number of scaling coefficient vectors used for different numbers of tasks.

	Preference weighted sum of accuracies (↑)						
# tasks	2	3	4	5	6	7	8
Single task models	75.84±1.76	77.03±1.84	82.43±4.40	87.69±4.50	88.52±4.02	89.26±3.58	90.62±2.52
MTL	73.63±0.30	75.13±1.00	80.10±2.79	84.93±3.58	86.78±2.94	87.40±2.56	89.11±2.36
Model soups ((Wortsman et al., 2022))	67.79±1.46	64.25±2.15	66.04±3.22	67.01±3.42	63.11±1.99	63.35±2.17	64.36±2.77
TIES-merging ((Yadav et al., 2024))	69.30±0.33	67.60±0.58	71.79±2.93	76.49±3.10	73.74±2.96	72.54±2.87	72.24±1.91
DARE-TIES	67.62±1.65	66.49±2.34	71.39±4.45	74.55±4.55	73.34±4.10	71.43±3.84	71.89±2.86
Task Arithmetic ((Ilharco et al., 2022))	**70.73±1.84**	61.15±2.33	52.69±4.23	61.58±4.62	51.37±3.84	39.79±3.97	60.77±2.84
TA with preference as weights	69.22±1.4	66.88±2.37	68.73±5.48	71.92±5.5	68.13±4.69	68.14±4.2	68.17±2.89
DARE-TA	70.61±0.22	64.18±1.24	58.04±8.19	65.39±7.03	56.76±7.01	46.75±5.73	64.51±3.81
Ada-Merging++ ((Yang et al., 2024))	67.27±1.92	67.13±1.92	71.19±4.43	76.84±4.71	74.13±4.07	72.58±4.16	72.55±2.83
DELLA-Merging ((Deep et al., 2024))	67.10±2.08	65.92±2.48	70.71±4.31	74.43±4.32	72.64±3.77	71.16±3.95	71.49±2.83
MOEA/D	70.22 ± 1.46	67.94 ± 1.79	70.85 ± 4.58	72.03 ± 4.03	67.88 ± 3.09	69.06 ± 2.97	68.59 ± 2.89
MAP	70.70±1.76	**69.05±1.84**	**72.84±4.40**	**77.31±4.50**	**74.26±4.02**	**73.40±3.58**	**72.96±2.52**

5 Related Work

Due to space constraints, for a more comprehensive discussion, please refer to Appendix B.

Multi-objective optimization Multi-objective optimization identifies diverse Pareto solutions with different trade-offs. The multi-task problem has been approached from a MOOP perspective (Sener & Koltun, 2018; Lin et al., 2019), utilizing algorithms like MGDA, IMTL, GradNorm, RLW, and scalarization. While these methods iteratively optimize $\mathbb{R}^d$ model parameters with significant computational cost, our approach performs post-training MOOP over $\mathbb{R}^N$ scaling coefficients, reducing computational burden. For $N \geq 3$ objectives, MOOP becomes many-objective optimization, challenging traditional algorithms (e.g. NSGA-II and SPEA2). Advanced methods such as ϵ-MOEA (Deb et al., 2003), MSOPS (Hughes, 2005), SMS-EMOA (Beume et al., 2007), and NSGA-III (Deb & Jain, 2013), or the KKT approach (Augusto et al., 2014) are required.

Task arithmetic Task arithmetic, a model merging method gaining attention, uses weighted averages of models for multi-task performance. Various approaches exist for selecting scaling coefficients: Ilharco et al. (2022) used equal scaling, which is suboptimal and limited; Yang et al. (2023) optimized weights using Shannon entropy but required unlabeled test data, which conflict with data privacy goals in model merging. Beyond task arithmetic, Ainsworth et al. (2023) merge models via weight matrix permutations, even without shared pretraining. Jin et al. (2023) introduced dataless knowledge fusion. Daheim et al. (2024) proposed uncertainty-based gradient matching for improved merging performance and robustness.

6 Conclusion and Limitations

We introduced MAP, a novel low-compute approach to efficiently merge models while accounting for trade-offs between multiple tasks. By leveraging a quadratic approximation of the evaluation metrics, MAP successfully identifies amortized Pareto fronts without the need for gradient descent for deep neural networks. The algorithm's efficiency is further enhanced through Bayesian adaptive sampling and nested merging, enabling it to scale to problems with a higher number of tasks. Moreover, MAP is an out-of-the-box plug-in for other task-vector-based model merging methods.

However, we would like to point out some limitations of our method. We do not have a detector algorithm to detect if two tasks have proper trade-offs. Approximating a Pareto "front" with only a single Pareto solution can lead to degenerate solutions. In this case, practitioners should be informed.

REFERENCES

Samuel K. Ainsworth, Jonathan Hayase, and Siddhartha S. Srinivasa. Git re-basin: Merging models modulo permutation symmetries. In *The Eleventh International Conference on Learning Representations, ICLR 2023, Kigali, Rwanda, May 1-5, 2023*. OpenReview.net, 2023. URL `https://openreview.net/pdf?id=CQsmMYmlP5T`.

Zeyuan Allen-Zhu, Yuanzhi Li, and Zhao Song. A convergence theory for deep learning via over-parameterization. In *International conference on machine learning*, pp. 242–252. PMLR, 2019.

Oscar Brito Augusto, Fouad Bennis, Stephane Caro, et al. Multiobjective optimization involving quadratic functions. *Journal of optimization*, 2014, 2014.

Nicola Beume, Boris Naujoks, and Michael Emmerich. Sms-emoa: Multiobjective selection based on dominated hypervolume. *European Journal of Operational Research*, 181(3):1653–1669, 2007.

Tom Brown, Benjamin Mann, Nick Ryder, Melanie Subbiah, Jared D Kaplan, Prafulla Dhariwal, Arvind Neelakantan, Pranav Shyam, Girish Sastry, Amanda Askell, et al. Language models are few-shot learners. *Advances in neural information processing systems*, 33:1877–1901, 2020.

Zhiqi Bu, Xinwei Zhang, Mingyi Hong, Sheng Zha, and George Karypis. Pre-training differentially private models with limited public data. *arXiv preprint arXiv:2402.18752*, 2024.

Sébastien Bubeck et al. Convex optimization: Algorithms and complexity. *Foundations and Trends® in Machine Learning*, 8(3-4):231–357, 2015.

Gong Cheng, Junwei Han, and Xiaoqiang Lu. Remote sensing image scene classification: Benchmark and state of the art. *Proceedings of the IEEE*, 105(10):1865–1883, 2017.

Lenaic Chizat, Edouard Oyallon, and Francis Bach. On lazy training in differentiable programming. *Advances in neural information processing systems*, 32, 2019.

Mircea Cimpoi, Subhransu Maji, Iasonas Kokkinos, Sammy Mohamed, and Andrea Vedaldi. Describing textures in the wild. In *Proceedings of the IEEE conference on computer vision and pattern recognition*, pp. 3606–3613, 2014.

Carlos A Coello Coello and Nareli Cruz Cortés. Solving multiobjective optimization problems using an artificial immune system. *Genetic programming and evolvable machines*, 6:163–190, 2005.

Haotian Cui, Chloe Wang, Hassaan Maan, Kuan Pang, Fengning Luo, Nan Duan, and Bo Wang. scgpt: toward building a foundation model for single-cell multi-omics using generative ai. *Nature Methods*, pp. 1–11, 2024.

Nico Daheim, Thomas Möllenhoff, Edoardo Ponti, Iryna Gurevych, and Mohammad Emtiyaz Khan. Model merging by uncertainty-based gradient matching. In *The Twelfth International Conference on Learning Representations*, 2024. URL `https://openreview.net/forum?id=D7KJmfEDQP`.

Kalyanmoy Deb and Himanshu Jain. An evolutionary many-objective optimization algorithm using reference-point-based nondominated sorting approach, part i: solving problems with box constraints. *IEEE transactions on evolutionary computation*, 18(4):577–601, 2013.

Kalyanmoy Deb, Manikanth Mohan, and Shikhar Mishra. Towards a quick computation of well-spread pareto-optimal solutions. In *Evolutionary Multi-Criterion Optimization: Second International Conference, EMO 2003, Faro, Portugal, April 8–11, 2003. Proceedings 2*, pp. 222–236. Springer, 2003.

Pala Tej Deep, Rishabh Bhardwaj, and Soujanya Poria. Della-merging: Reducing interference in model merging through magnitude-based sampling. *arXiv preprint arXiv: 2406.11617*, 2024.

Alexey Dosovitskiy, Lucas Beyer, Alexander Kolesnikov, Dirk Weissenborn, Xiaohua Zhai, Thomas Unterthiner, Mostafa Dehghani, Matthias Minderer, Georg Heigold, Sylvain Gelly, et al. An image is worth 16x16 words: Transformers for image recognition at scale. *arXiv preprint arXiv:2010.11929*, 2020.

Guodong Du, Jing Li, Hanting Liu, Runhua Jiang, Shuyang Yu, Yifei Guo, S. Goh, and Ho-Kin Tang. Knowledge fusion by evolving weights of language models. *Annual Meeting of the Association for Computational Linguistics*, 2024. doi: 10.48550/arXiv.2406.12208.

Simon Du, Jason Lee, Haochuan Li, Liwei Wang, and Xiyu Zhai. Gradient descent finds global minima of deep neural networks. In *International conference on machine learning*, pp. 1675–1685. PMLR, 2019.

Saeed Ghadimi and Guanghui Lan. Stochastic first-and zeroth-order methods for nonconvex stochastic programming. *SIAM journal on optimization*, 23(4):2341–2368, 2013.

Kaiming He, Xiangyu Zhang, Shaoqing Ren, and Jian Sun. Deep residual learning for image recognition. In *Proceedings of the IEEE conference on computer vision and pattern recognition*, pp. 770–778, 2016.

Patrick Helber, Benjamin Bischke, Andreas Dengel, and Damian Borth. Eurosat: A novel dataset and deep learning benchmark for land use and land cover classification. *IEEE Journal of Selected Topics in Applied Earth Observations and Remote Sensing*, 12(7):2217–2226, 2019.

Jordan Hoffmann, Sebastian Borgeaud, Arthur Mensch, Elena Buchatskaya, Trevor Cai, Eliza Rutherford, Diego de Las Casas, Lisa Anne Hendricks, Johannes Welbl, Aidan Clark, et al. Training compute-optimal large language models. *arXiv preprint arXiv:2203.15556*, 2022.

Evan J Hughes. Evolutionary many-objective optimisation: many once or one many? In *2005 IEEE congress on evolutionary computation*, volume 1, pp. 222–227. IEEE, 2005.

Gabriel Ilharco, Marco Tulio Ribeiro, Mitchell Wortsman, Suchin Gururangan, Ludwig Schmidt, Hannaneh Hajishirzi, and Ali Farhadi. Editing models with task arithmetic. *arXiv preprint arXiv:2212.04089*, 2022.

Gabriel Ilharco, Marco Túlio Ribeiro, Mitchell Wortsman, Ludwig Schmidt, Hannaneh Hajishirzi, and Ali Farhadi. Editing models with task arithmetic. In *The Eleventh International Conference on Learning Representations, ICLR 2023, Kigali, Rwanda, May 1-5, 2023*. OpenReview.net, 2023. URL `https://openreview.net/pdf?id=6t0Kwf8-jrj`.

Moksh Jain, Emmanuel Bengio, Alex Hernández-García, Jarrid Rector-Brooks, Bonaventure F. P. Dossou, Chanakya Ajit Ekbote, Jie Fu, Tianyu Zhang, Michael Kilgour, Dinghuai Zhang, Lena Simine, Payel Das, and Yoshua Bengio. Biological sequence design with gflownets. In Kamalika Chaudhuri, Stefanie Jegelka, Le Song, Csaba Szepesvári, Gang Niu, and Sivan Sabato (eds.), *International Conference on Machine Learning, ICML 2022, 17-23 July 2022, Baltimore, Maryland, USA*, volume 162 of *Proceedings of Machine Learning Research*, pp. 9786–9801. PMLR, 2022. URL `https://proceedings.mlr.press/v162/jain22a.html`.

Joel Jang, Seungone Kim, Bill Yuchen Lin, Yizhong Wang, Jack Hessel, Luke Zettlemoyer, Hannaneh Hajishirzi, Yejin Choi, and Prithviraj Ammanabrolu. Personalized soups: Personalized large language model alignment via post-hoc parameter merging. *arXiv preprint arXiv: 2310.11564*, 2023.

Albert Q. Jiang, Alexandre Sablayrolles, Antoine Roux, Arthur Mensch, Blanche Savary, Chris Bamford, Devendra Singh Chaplot, Diego de las Casas, Emma Bou Hanna, Florian Bressand, Gianna Lengyel, Guillaume Bour, Guillaume Lample, Lélio Renard Lavaud, Lucile Saulnier, Marie-Anne Lachaux, Pierre Stock, Sandeep Subramanian, Sophia Yang, Szymon Antoniak, Teven Le Scao, Théophile Gervet, Thibaut Lavril, Thomas Wang, Timothée Lacroix, and William El Sayed. Mixtral of experts. *arXiv preprint arXiv: 2401.04088*, 2024.

Xisen Jin, Xiang Ren, Daniel Preotiuc-Pietro, and Pengxiang Cheng. Dataless knowledge fusion by merging weights of language models. In *The Eleventh International Conference on Learning Representations, ICLR 2023, Kigali, Rwanda, May 1-5, 2023*. OpenReview.net, 2023. URL `https://openreview.net/forum?id=FCnohuR6AnM`.

Jared Kaplan, Sam McCandlish, Tom Henighan, Tom B Brown, Benjamin Chess, Rewon Child, Scott Gray, Alec Radford, Jeffrey Wu, and Dario Amodei. Scaling laws for neural language models. *arXiv preprint arXiv:2001.08361*, 2020.

Jonathan Krause, Michael Stark, Jia Deng, and Li Fei-Fei. 3d object representations for fine-grained categorization. In *Proceedings of the IEEE international conference on computer vision workshops*, pp. 554–561, 2013.

Alex Krizhevsky, Geoffrey Hinton, et al. Learning multiple layers of features from tiny images. 2009.

Yann LeCun. The mnist database of handwritten digits. *http://yann. lecun. com/exdb/mnist/*, 1998.

Bingdong Li, Zixiang Di, Yanting Yang, Hong Qian, Peng Yang, Hao Hao, Ke Tang, and Aimin Zhou. It's morphing time: Unleashing the potential of multiple llms via multi-objective optimization. *arXiv preprint arXiv: 2407.00487*, 2024.

Xi Lin, Hui-Ling Zhen, Zhenhua Li, Qing-Fu Zhang, and Sam Kwong. Pareto multi-task learning. *Advances in neural information processing systems*, 32, 2019.

Xi Lin, Zhiyuan Yang, Qingfu Zhang, and Sam Kwong. Controllable pareto multi-task learning. *arXiv preprint arXiv: 2010.06313*, 2020.

Sam McCandlish, Jared Kaplan, Dario Amodei, and OpenAI Dota Team. An empirical model of large-batch training. *arXiv preprint arXiv:1812.06162*, 2018.

Henry B. Moss, David S. Leslie, Daniel Beck, Javier Gonzalez, and Paul Rayson. Boss: Bayesian optimization over string spaces. In *Advances in Neural Information Processing Systems*, 2020. URL `https://proceedings.neurips.cc/paper/2020/hash/b19aa25ff58940d974234b48391b9549-Abstract.html`.

Aviv Navon, Aviv Shamsian, Gal Chechik, and Ethan Fetaya. Learning the pareto front with hypernetworks. *arXiv preprint arXiv: 2010.04104*, 2020.

Yuval Netzer, Tao Wang, Adam Coates, Alessandro Bissacco, Baolin Wu, Andrew Y Ng, et al. Reading digits in natural images with unsupervised feature learning. In *NIPS workshop on deep learning and unsupervised feature learning*, volume 2011, pp. 7. Granada, Spain, 2011.

Maria-Elena Nilsback and Andrew Zisserman. Automated flower classification over a large number of classes. In *2008 Sixth Indian conference on computer vision, graphics & image processing*, pp. 722–729. IEEE, 2008.

National Institutes of Health et al. Nih clinical center provides one of the largest publicly available chest x-ray datasets to scientific community, 2017.

E. O. Pyzer-Knapp. Bayesian optimization for accelerated drug discovery. *IBM Journal of Research and Development*, 62(6):2:1–2:7, 2018. doi: 10.1147/JRD.2018.2881731.

Alec Radford, Jong Wook Kim, Chris Hallacy, Aditya Ramesh, Gabriel Goh, Sandhini Agarwal, Girish Sastry, Amanda Askell, Pamela Mishkin, Jack Clark, et al. Learning transferable visual models from natural language supervision. In *International conference on machine learning*, pp. 8748–8763. PMLR, 2021.

Alexandre Ram'e, Nino Vieillard, L'eonard Hussenot, Robert Dadashi, Geoffrey Cideron, Olivier Bachem, and Johan Ferret. Warm: On the benefits of weight averaged reward models. *International Conference on Machine Learning*, 2024. doi: 10.48550/arXiv.2401.12187.

Alexandre Ramé, Guillaume Couairon, Mustafa Shukor, Corentin Dancette, Jean-Baptiste Gaya, L. Soulier, and M. Cord. Rewarded soups: towards pareto-optimal alignment by interpolating weights fine-tuned on diverse rewards. *Neural Information Processing Systems*, 2023. doi: 10.48550/arXiv.2306.04488.

Alexandre Ramé, Johan Ferret, Nino Vieillard, Robert Dadashi, Léonard Hussenot, Pierre-Louis Cedoz, Pier Giuseppe Sessa, Sertan Girgin, Arthur Douillard, and Olivier Bachem. Warp: On the benefits of weight averaged rewarded policies. *arXiv preprint arXiv: 2406.16768*, 2024.

Baptiste Rozière, Jonas Gehring, Fabian Gloeckle, Sten Sootla, Itai Gat, Xiaoqing Ellen Tan, Yossi Adi, Jingyu Liu, Romain Sauvestre, Tal Remez, Jérémy Rapin, Artyom Kozhevnikov, Ivan Evtimov, Joanna Bitton, Manish Bhatt, Cristian Canton Ferrer, Aaron Grattafiori, Wenhan Xiong, Alexandre Défossez, Jade Copet, Faisal Azhar, Hugo Touvron, Louis Martin, Nicolas Usunier, Thomas Scialom, and Gabriel Synnaeve. Code llama: Open foundation models for code. *arXiv preprint arXiv: 2308.12950*, 2023.

Michael Ruchte and Josif Grabocka. Scalable pareto front approximation for deep multi-objective learning. *2021 IEEE International Conference on Data Mining (ICDM)*, pp. 1306–1311, 2021. doi: 10.1109/ICDM51629.2021.00162.

Ozan Sener and Vladlen Koltun. Multi-task learning as multi-objective optimization. In S. Bengio, H. Wallach, H. Larochelle, K. Grauman, N. Cesa-Bianchi, and R. Garnett (eds.), *Advances in Neural Information Processing Systems*, volume 31. Curran Associates, Inc., 2018. URL https://proceedings.neurips.cc/paper_files/paper/2018/file/432aca3a1e345e339f35a30c8f65edce-Paper.pdf.

Ken Shoemake. Animating rotation with quaternion curves. In *Proceedings of the 12th Annual Conference on Computer Graphics and Interactive Techniques*, SIGGRAPH '85, pp. 245–254, New York, NY, USA, 1985. Association for Computing Machinery. ISBN 0897911660. doi: 10.1145/325334.325242. URL https://doi.org/10.1145/325334.325242.

Johannes Stallkamp, Marc Schlipsing, Jan Salmen, and Christian Igel. The german traffic sign recognition benchmark: a multi-class classification competition. In *The 2011 international joint conference on neural networks*, pp. 1453–1460. IEEE, 2011.

Hui Su, Zhi Tian, Xiaoyu Shen, and Xunliang Cai. Unraveling the mystery of scaling laws: Part i. *arXiv preprint arXiv:2403.06563*, 2024.

Kei Terayama, Masato Sumita, Ryo Tamura, and Koji Tsuda. Black-box optimization for automated discovery. *Accounts of Chemical Research*, 54(6):1334–1346, 2021.

Arun James Thirunavukarasu, Darren Shu Jeng Ting, Kabilan Elangovan, Laura Gutierrez, Ting Fang Tan, and Daniel Shu Wei Ting. Large language models in medicine. *Nature medicine*, 29(8): 1930–1940, 2023.

Hugo Touvron, Louis Martin, Kevin Stone, Peter Albert, Amjad Almahairi, Yasmine Babaei, Nikolay Bashlykov, Soumya Batra, Prajjwal Bhargava, Shruti Bhosale, Dan Bikel, Lukas Blecher, Cristian Canton Ferrer, Moya Chen, Guillem Cucurull, David Esiobu, Jude Fernandes, Jeremy Fu, Wenyin Fu, Brian Fuller, Cynthia Gao, Vedanuj Goswami, Naman Goyal, Anthony Hartshorn, Saghar Hosseini, Rui Hou, Hakan Inan, Marcin Kardas, Viktor Kerkez, Madian Khabsa, Isabel Kloumann, Artem Korenev, Punit Singh Koura, Marie-Anne Lachaux, Thibaut Lavril, Jenya Lee, Diana Liskovich, Yinghai Lu, Yuning Mao, Xavier Martinet, Todor Mihaylov, Pushkar Mishra, Igor Molybog, Yixin Nie, Andrew Poulton, Jeremy Reizenstein, Rashi Rungta, Kalyan Saladi, Alan Schelten, Ruan Silva, Eric Michael Smith, Ranjan Subramanian, Xiaoqing Ellen Tan, Binh Tang, Ross Taylor, Adina Williams, Jian Xiang Kuan, Puxin Xu, Zheng Yan, Iliyan Zarov, Yuchen Zhang, Angela Fan, Melanie Kambadur, Sharan Narang, Aurelien Rodriguez, Robert Stojnic, Sergey Edunov, and Thomas Scialom. Llama 2: Open foundation and fine-tuned chat models. *arXiv preprint arXiv: 2307.09288*, 2023.

David Allen Van Veldhuizen. *Multiobjective evolutionary algorithms: classifications, analyses, and new innovations*. Air Force Institute of Technology, 1999.

Haoxiang Wang, Yong Lin, Wei Xiong, Rui Yang, Shizhe Diao, Shuang Qiu, Han Zhao, and Tong Zhang. Arithmetic control of llms for diverse user preferences: Directional preference alignment with multi-objective rewards. *arXiv preprint arXiv: 2402.18571*, 2024a.

Xiaosong Wang, Yifan Peng, Le Lu, Zhiyong Lu, Mohammadhadi Bagheri, and Ronald M Summers. Chestx-ray8: Hospital-scale chest x-ray database and benchmarks on weakly-supervised classification and localization of common thorax diseases. In *Proceedings of the IEEE conference on computer vision and pattern recognition*, 2017.

Yibo Wang, Sijia Chen, Wei Jiang, Wenhao Yang, Yuanyu Wan, and Lijun Zhang. Online composite optimization between stochastic and adversarial environments. In *In Advances in Neural Information Processing Systems 37 (NeurIPS 2024)*, 2024b.

James T. Wilson, Riccardo Moriconi, Frank Hutter, and Marc Peter Deisenroth. The reparameterization trick for acquisition functions, 2017.

Michael Wornow, Rahul Thapa, Ethan Steinberg, Jason Fries, and Nigam Shah. Ehrshot: An ehr benchmark for few-shot evaluation of foundation models. 2023.

Mitchell Wortsman, Gabriel Ilharco, S. Gadre, R. Roelofs, Raphael Gontijo-Lopes, Ari S. Morcos, Hongseok Namkoong, Ali Farhadi, Y. Carmon, Simon Kornblith, and Ludwig Schmidt. Model soups: averaging weights of multiple fine-tuned models improves accuracy without increasing inference time. *International Conference on Machine Learning*, 2022. doi: 10.48550/arXiv.2203.05482.

Yusong Wu, Ke Chen, Tianyu Zhang, Yuchen Hui, Taylor Berg-Kirkpatrick, and Shlomo Dubnov. Large-scale contrastive language-audio pretraining with feature fusion and keyword-to-caption augmentation. In *IEEE International Conference on Acoustics, Speech and Signal Processing ICASSP 2023, Rhodes Island, Greece, June 4-10, 2023*, pp. 1–5. IEEE, 2023. doi: 10.1109/ICASSP49357.2023.10095969. URL https://doi.org/10.1109/ICASSP49357.2023.10095969.

Jianxiong Xiao, Krista A Ehinger, James Hays, Antonio Torralba, and Aude Oliva. Sun database: Exploring a large collection of scene categories. *International Journal of Computer Vision*, 119: 3–22, 2016.

Prateek Yadav, Derek Tam, Leshem Choshen, Colin Raffel, and Mohit Bansal. Ties-merging: Resolving interference when merging models. *Neural Information Processing Systems*, 2023.

Prateek Yadav, Derek Tam, Leshem Choshen, Colin A Raffel, and Mohit Bansal. Ties-merging: Resolving interference when merging models. *Advances in Neural Information Processing Systems*, 36, 2024.

Enneng Yang, Zhenyi Wang, Li Shen, Shiwei Liu, Guibing Guo, Xingwei Wang, and Dacheng Tao. Adamerging: Adaptive model merging for multi-task learning. *arXiv preprint arXiv:2310.02575*, 2023.

Enneng Yang, Zhenyi Wang, Li Shen, Shiwei Liu, Guibing Guo, Xingwei Wang, and Dacheng Tao. Adamerging: Adaptive model merging for multi-task learning. In *The Twelfth International Conference on Learning Representations*, 2024. URL https://openreview.net/forum?id=nZP6NgD3QY.

Le Yu, Bowen Yu, Haiyang Yu, Fei Huang, and Yongbin Li. Language models are super mario: Absorbing abilities from homologous models as a free lunch. *arXiv preprint arXiv:2311.03099*, 2023.

Xiaohua Zhai, Basil Mustafa, Alexander Kolesnikov, and Lucas Beyer. Sigmoid loss for language image pre-training. *IEEE International Conference on Computer Vision*, 2023. doi: 10.1109/ICCV51070.2023.01100.

Qingfu Zhang and Hui Li. Moea/d: A multiobjective evolutionary algorithm based on decomposition. *IEEE Transactions on evolutionary computation*, 11(6):712–731, 2007.

Yifan Zhong, Chengdong Ma, Xiaoyuan Zhang, Ziran Yang, Haojun Chen, Qingfu Zhang, Siyuan Qi, and Yaodong Yang. Panacea: Pareto alignment via preference adaptation for llms. *arXiv preprint arXiv: 2402.02030*, 2024.

Zhanhui Zhou, Jie Liu, Chao Yang, Jing Shao, Yu Liu, Xiangyu Yue, Wanli Ouyang, and Yu Qiao. Beyond one-preference-fits-all alignment: Multi-objective direct preference optimization. *arXiv preprint arXiv: 2310.03708*, 2023.

Contents

A Notations

For clarity, we summarize the notations used throughout the paper in Table 5.

Table 5: Table of notations.

Notations	**Explanation**
N	Number of tasks
$\mathbf{c}$	Vector of scaling coefficients for task vectors
c_n	Scaling coefficients for the nth task
$\boldsymbol{\theta}_{\text{pre}}$	Pretrained model parameters
$\theta_m(\mathbf{c})$	Merged model parameters as a function of scaling vector $\mathbf{c}$
$\mathbf{v_n}$	Task vector for task n
$\mathbf{V}$	Task matrix formed by concatenating task vectors
$M_n(\mathbf{c})$	Evaluation metric for task n as a function of $\mathbf{c}$
$\mathbf{A}_n$	Quadratic coefficient matrix in the surrogate model
$\mathbf{b}_n$	Linear coefficient vector in the surrogate model
e_n	Constant term in the surrogate model
$\tilde{M}_n(\mathbf{c}; \mathbf{A}_n, \mathbf{b}_n, e_n)$	Surrogate quadratic model for task n
Ω	Set of scaling coefficient vectors $\mathbf{c}$ used for estimating surrogate model parameters
K	Number of sampled coefficient vectors in set Ω

B More Discussion on Related Work

Second-order Taylor expansion In deep learning, the second-order Taylor expansion and thus the quadratic approximation on the evaluation metric is an important technique, that characterizes the metric landscape. For example, the Newton-Ralphson method is derived from it: $\mathbf{w}_t - \mathbf{w}_{t+1} = \mathbf{H}^{-1}\mathbf{G} = \text{argmin}_{\mathbf{v}} M(\mathbf{w}_t - \mathbf{v})$ given that $M(\mathbf{w}_t - \mathbf{v}) = M(\mathbf{w}_t) - \mathbf{v}\mathbf{G} + \frac{1}{2}\mathbf{v}^\top\mathbf{H}\mathbf{v}$. The quadratic approximation is also combined with Lipschitz smoothness (L) in the classic convergence analysis of SGD (Bubeck et al., 2015; Ghadimi & Lan, 2013), through $M(\mathbf{w}_t - \eta\mathbf{G}) \leq M(\mathbf{w}_t) - \eta||\mathbf{G}||^2 + \frac{L\eta^2}{2}||\mathbf{G}||^2$. Interestingly, although the approximation is only accurate in the local neighborhood, it can be used to indicate the global convergence over the iterations. One reason is that state-of-the-art neural networks are usually over-parameterized and undergo lazy training, meaning that the converging parameters are close to the initialization (Chizat et al., 2019; Du et al., 2019; Allen-Zhu et al., 2019). Thus, the local approximation informs the global convergence behavior. In particular, this approximation has played important roles in the scaling laws of neural networks (e.g. Equation 3.3 in (Su et al., 2024)) that predict the performance and help select hyperparameters before training actually takes place.

Pareto fronts for Multi-task Learning Recent advancements in multi-task learning (MTL) have seen diverse approaches to Pareto Front learning in machine learning. Sener & Koltun (2018) explicitly formulated multi-task learning as a multi-objective optimization problem and adapted gradient-based multi-objective optimization algorithms to large-scale learning problems. Lin et al. (2019) developed a constrained optimization approach to find multiple Pareto optimal solutions representing different trade-offs among tasks in multi-task learning and solved decomposed subproblems in parallel using gradient-based optimization. It requires separate training runs for each solution. Navon et al. (2020) and Lin et al. (2020) employed hypernetworks for continuous Pareto Front approximation, generating target network weights based on preferred trade-offs. However, the size of these hypernetworks can become prohibitively large and needs to be properly trained as well. Ruchte and Grabocka Ruchte & Grabocka (2021) introduced a memory-efficient method by augmenting network inputs with desired trade-offs, although this may obscure the network's conditioning due to nonlinear dynamics, and it is also based on the gradient updating method.

Model-merging Applications in LLM In the realm of model merging applications for language model preferences, recent research has made significant progress. Ramé et al. (2023) and Jang et al. (2023) introduced "rewarded soups" and "personalized soups", which utilize model soup to interpolate weights of networks fine-tuned on diverse rewards to achieve Pareto-optimal generalization across preference spaces and address the challenge of aligning large language models with individual perspectives. WARP (Weight Averaged Rewarded Policies) (Ramé et al., 2024) and WARM (Weight Averaged Reward Models) (Ram'e et al., 2024) demonstrate how merging policies or reward models in weight space can refine the trade-off between competing constraints, such as reward optimization and alignment with pre-trained knowledge or human preferences. (Zhong et al., 2024) developed “Panacea", which reframes alignment as a multi-dimensional preference optimization problem, using singular value decomposition-based low-rank adaptation to guide model behavior with a low-dimensional preference vector. To address the limitations of scalar rewards in RLHF, Zhou et al. (2023) introduced Multi-Objective Direct Preference Optimization, an RL-free algorithm that extends Direct Preference Optimization to handle multiple alignment objectives efficiently. Du et al. (2024) relies on “mutation" and crossover operations typical of evolutionary algorithms, exploring the parameter space by combining and perturbing existing solutions. Models are evaluated on development datasets, and only those that improve upon their predecessors are retained, guiding the population toward better-performing solutions. Li et al. (2024) employs Bayesian optimization with a weak-to-strong approach and utilizes Fisher information to improve the selection of configurations for evaluation, aiming to find optimal merging configurations within limited computational budgets. Wang et al. (2024b) investigated online learning with limited resources, and successfully deployed model aggregation to handle changing environments, establishing optimal theoretical guarantees. Finally, Wang et al. (2024a) proposed the Directional Preference Alignment framework, which incorporates multi-objective reward modeling to represent user preferences, offering intuitive arithmetic control over LLM generation for diverse user preferences.

Bayesian Optimization Bayesian optimization has been widely used in scenarios that require efficient exploration of parameter spaces, particularly when evaluating the performance of each configuration is costly or time-consuming. This method is especially advantageous in machine learning and hyperparameter tuning, where traditional optimization techniques may be computationally prohibitive (Wilson et al., 2017; Jain et al., 2022; Moss et al., 2020; Pyzer-Knapp, 2018; Terayama et al., 2021).

C Additional Details on the Methods

C.1 Proof: Negligibility of the Remainder in Multivariate Taylor Series

Corollary 2. *If $f : \mathbb{R}^n \to \mathbb{R}$ is $(k+1)$ times continuously differentiable in a neighborhood around a point $a \in \mathbb{R}^n$, then the Taylor polynomial $T_k(x)$ of order k provides an accurate approximation of $f(x)$ when x is sufficiently close to a. Furthermore, the remainder term $R_k(x)$ becomes negligibly small as $||x - a||$ approaches zero, assuming that the $(k+1)$th derivatives of f are bounded by a constant M in the neighborhood between a and x.*

Proof *Consider the Taylor series expansion of f around the point a, truncated at order k:*

$$T_k(x) = \sum_{|\alpha| \leq k} \frac{D^\alpha f(a)}{\alpha!}(x-a)^\alpha$$

where α is a multi-index of non-negative integers, $D^\alpha f(a)$ denotes the partial derivatives of f at a corresponding to α, and $(x-a)^\alpha = (x_1 - a_1)^{\alpha_1} \dots (x_n - a_n)^{\alpha_n}$.

Assumptions

1. *Proximity: $\|x - a\| \to 0$ where $\| \cdot \|$ denotes the Euclidean norm in $\mathbb{R}^n$.*
2. *Bounded Derivatives: There exists a constant M such that for all multi-indices α with $|\alpha| \equiv k+1$, the norm of the tensor $D^\alpha f$ evaluated at any point ξ between a and x is bounded by M.*

$$\|D^\alpha f(\xi)\| = \sup_{\|v_1\|=1,\dots,\|v_{k+1}\|=1} |D^\alpha f(\xi)(v_1, \dots, v_{k+1})| \leq M$$

The remainder term of the Taylor series expansion is given by:

$$R_k(x) = \sum_{|\alpha|=k+1} \frac{D^\alpha f(\xi)}{\alpha!}(x-a)^\alpha$$

Given the assumptions, we estimate:

$$|R_k(x)| \leq \sum_{|\alpha|=k+1} \frac{\|D^\alpha f(\xi)\|}{\alpha!}\|x-a\|^{k+1} \leq \sum_{|\alpha|=k+1} \frac{M}{\alpha!}\|x-a\|^{k+1}$$

As $\|x-a\| \to 0$, the term $\|x-a\|^{k+1}$ goes to zero. Thus, the remainder term $R_k(x)$ becomes arbitrarily small, making it negligible.

In conclusion, under the stated assumptions, the Taylor series truncated at order k, $T_k(x)$, provides an accurate approximation of $f(x)$ near a, and the remainder $R_k(x)$ can be ignored as $\|x-a\| \to 0$ and the higher-order derivatives remain bounded by M.

C.2 Closed-form Solution for Surrogate Model Parameters

Corollary 3 (Closed-form Solution for Surrogate Model Parameters)**.** *Under Assumption 1, for each task $n = 1, \ldots, N$, the optimization problem*

$$(A_n^*, \mathbf{b}_n^*, e_n^*) = \arg\min_{A_n, \mathbf{b}_n, e_n} \sum_{\mathbf{c}\in\Omega} \left| M_n\left(\theta_m(\mathbf{c})\right) - \tilde{M}_n(\mathbf{c}; A_n, \mathbf{b}_n, e_n)\right|^2$$

is equivalent to solving the following linear regression problem:

1. ***Predictors**: For each coefficient vector $\mathbf{c} = (c_1, c_2, \ldots, c_N)^\top \in \mathbb{R}^N$, construct the predictor vector $\mathbf{C}_n(\mathbf{c}) \in \mathbb{R}^{\frac{N(N+3)}{2}+1}$ as*

   $$\mathbf{C}_n(\mathbf{c}) = [c_1^2, c_2^2, \ldots, c_N^2, c_1c_2, c_1c_3, \ldots, c_{N-1}c_N, c_1, c_2, \ldots, c_N, 1]$$

   This vector includes:

   - *Quadratic terms: c_i^2 for $i = 1, \ldots, N$.*
   - *Interaction terms: c_ic_j for $1 \leq i < j \leq N$.*
   - *Linear terms: c_i for $i = 1, \ldots, N$.*
   - *Constant term: 1.*

2. ***Response Variable**: Let $\mathbf{y}_n \in \mathbb{R}^K$ be the vector of observed evaluation metrics for task n across all sampled coefficients $\Omega = \{\mathbf{c}^{(1)}, \ldots, \mathbf{c}^{(K)}\}$:*

   $$\mathbf{y}_n = \begin{bmatrix} M_n\left(\theta_m(\mathbf{c}^{(1)})\right) \\ M_n\left(\theta_m(\mathbf{c}^{(2)})\right) \\ \vdots \\ M_n\left(\theta_m(\mathbf{c}^{(K)})\right) \end{bmatrix}$$

3. ***Design Matrix**: Construct the design matrix $\mathbf{C}_n \in \mathbb{R}^{K\times\left(\frac{N(N+3)}{2}+1\right)}$ where each row corresponds to $\mathbf{C}_n(\mathbf{c}^{(k)})^\top$ for $k = 1, \ldots, K$.*

4. ***Coefficient Vector**: Define the coefficient vector $\boldsymbol{\beta}_n \in \mathbb{R}^{\frac{N(N+3)}{2}+1}$ as*

   $$\boldsymbol{\beta}_n = \begin{bmatrix} vec(A_n) \\ \mathbf{b}_n \\ e_n \end{bmatrix}$$

   where $vec(A_n)$ represents the vectorization of the upper triangular part of A_n, including the diagonal elements.

***Optimal Solution**: The parameters $(A_n^*, \mathbf{b}_n^*, e_n^*)$ that minimize the mean squared error are obtained via the Ordinary Least Squares (OLS) solution:*

$$\boldsymbol{\beta}_n^* = \left(\mathbf{C}_n^\top \mathbf{C}_n\right)^{-1} \mathbf{C}_n^\top \mathbf{y}_n$$

***Interpretation**: This closed-form solution provides the optimal surrogate model parameters by fitting a quadratic model to the observed evaluation metrics through linear regression. The design matrix $\mathbf{C}_n$ incorporates all necessary quadratic, interaction, linear, and constant terms, enabling the surrogate model $\tilde{M}_n(\mathbf{c}; A_n, \mathbf{b}_n, e_n)$ to accurately approximate $M_n(\theta_m(\mathbf{c}))$ within the specified region.*

D Additional Details on Experiments

D.1 Experiment setup

Table 6: Experiment setup in terms of task details and models.

Task type	Metric	# of total tasks	Model type
Zero-shot Classification (normal)	Accuracy	8	ViT-B/32 (CLIP) ((Dosovitskiy et al., 2020))
Zero-shot Classification (medical)	Accuracy	2	ViT-B/32 (CLIP) ((Dosovitskiy et al., 2020))
Language Generation	Loss/Perplexity	4	Llama3-8B ((Touvron et al., 2023))
Image Classification	Accuracy	3	ResNet-18 ((He et al., 2016))

D.2 Additional metric: Generational distance and inverted generational distance

We evaluated the quality of the Pareto front in capturing the shape of the ground truth Pareto front by measuring how much the predicted Pareto front converges to the ground truth Pareto front by calculating the generational distance (GD) (Van Veldhuizen, 1999) and how much the predicted Pareto front covers the ground truth Pareto front by calculating the inverted generational distance (IGD) (Coello & Cortés, 2005). GD and IGD are standard measures used in evolutionary multi-objective optimization to evaluate the solutions found by the evolutionary algorithms. Given a predicted Pareto solution sets $PF_1 = \{(\tilde{M_1^j}(\theta_{merged}(\mathbf{c})), \ldots, \tilde{M_N^j}(\theta_{merged}(\mathbf{c}))) \mid j = 1, 2, \ldots, K_1\}$, and a ground truth Pareto solution sets $PF_2 = \{(M_1^j(\theta_{merged}(\mathbf{c})), \ldots, M_N^j(\theta_{merged}(\mathbf{c}))) \mid j = 1, 2, \ldots, K_2\}$ the GD and IGD metrics are defined as

$$GD(PF_1) \equiv \frac{1}{K_1}\left(\sum_{i=1}^{K_1} d_i^p\right)^{1/p} \text{ and } IGD(PF_1) \equiv \frac{1}{K_2}\left(\sum_{i=1}^{K_2} \tilde{d_i^p}\right)^{1/p}$$

where d_i is the minimal Euclidean distance from a specific Pareto Solution in PF_1 to PF_2 and $\tilde{d}_i$ is the minimal Euclidean distance from a specific Pareto Solution in PF_2 to PF_1.

Since the Pareto front that resulted from the direct search method when the number of tasks is low (i.e. strictly smaller than 4) can be deemed as ground truth Pareto fronts, we computed GD and IGD to compare the Pareto fronts produced by MAP against those obtained via brute-force grid search.

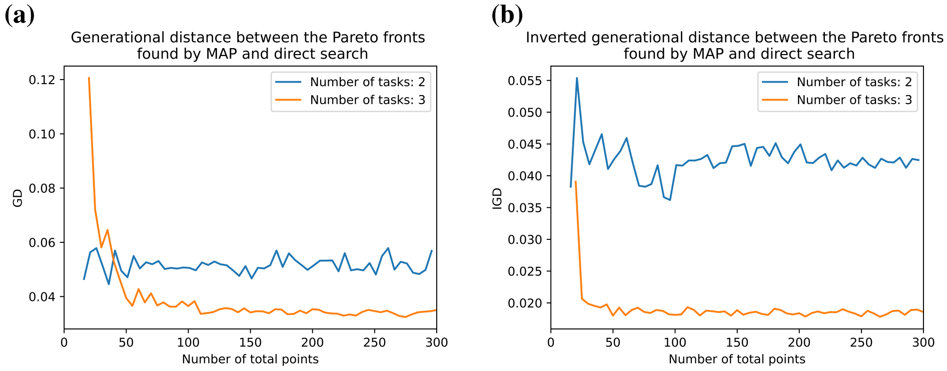

Figure 6: (a) Generational distance between the Pareto fronts by MAP and by direct search for dimensions 2 and 3. (b) Inverted generational distance between the Pareto fronts by MAP and by direct search for dimensions 2 and 3. For both subfigures, the x-axis is the number of total scaling coefficients used by MAP. For dimension 2, direct search used 200 scaling coefficients, and 300 for dimension 3.

D.3 Zero-shot Medical Image Classification

In addition to natural images, we used another dataset consisting of over 112,000 chest X-rays and 30,000 unique patients (of Health et al., 2017). It originally contained 15 classes (14 diseases and 1 class for no finding). We split the dataset into two groups, where medical task 1 specifically tries to classify Atelectasis, Consolidation, Infiltration, Pneumothorax, and medical task 2 tries to classify Nodule, Mass, and Hernia. An example image taken from the dataset is shown in Figure 7 (a).

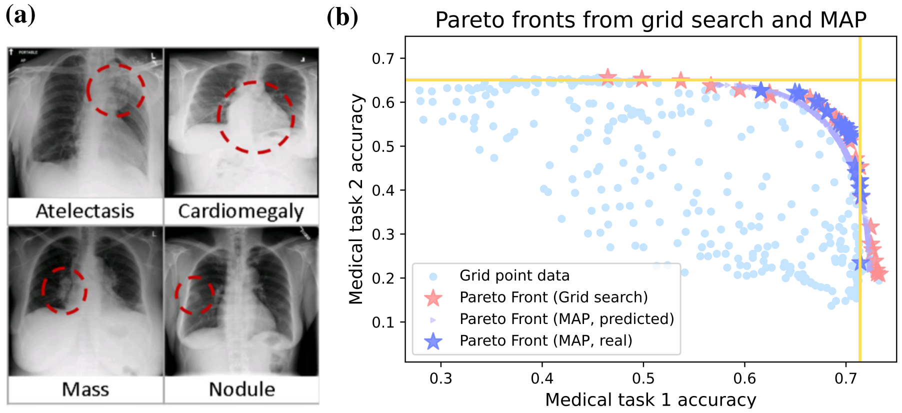

Figure 7: (a) Example figure from the NIH (of Health et al., 2017) dataset. (b) Pareto fronts found by brute-force direct search using 400 points and by MAP using 30 points. We randomly sampled 25 points from the predicted Pareto front by MAP. The resulting IGD is 0.016, and GD is 0.014.

D.4 Merging Language Model

Merging Languages We merge Llama-3-8B language models in French[3] and Arabic[4], as well as Chinese[5] and Japanese[6], as shown in Table 7. The ground truth Pareto front, however, exhibits significant limitations. It contains only a sparse set of points, indicating that few merged models dominate the rest. This also suggests that the trade-off between metrics across different languages

[3] https://huggingface.co/jpacifico/French-Alpaca-Llama3-8B-Instruct-v1.0
[4] https://huggingface.co/MohamedRashad/Arabic-Orpo-Llama-3-8B-Instruct
[5] https://huggingface.co/shenzhi-wang/Llama3-8B-Chinese-Chat
[6] https://huggingface.co/haqishen/Llama-3-8B-Japanese-Instruct

is not substantial. Despite these challenges, our algorithm successfully identifies the Pareto fronts. Please refer to Table 7 and Appendix D.4 for GD and IGD metrics between the Pareto fronts find by Grid Search and find by MAP and a visualization of the Pareto fronts found by MAP.

Furthermore, we experimented with merging Arabic+French and Chinese+Japanese using the nested scheme described in Algorithm 2, while considering various preference settings. However, the resulting Pareto front typically contains only a single model. This sparsity hinders our ability to effectively characterize a meaningful Pareto front in such scenarios.

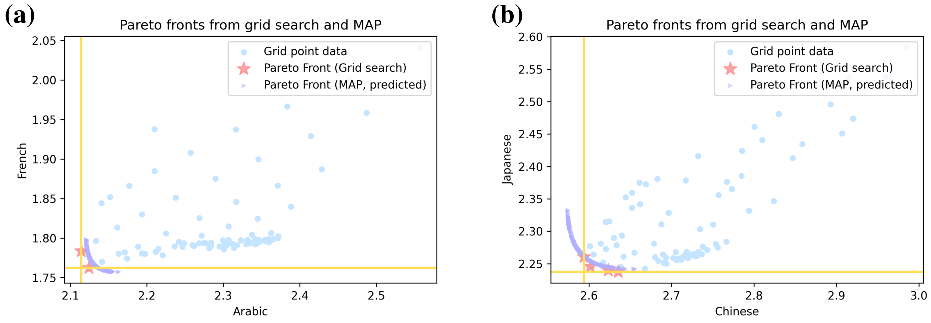

Figure 8: (a) Amortized Pareto front by MAP on merging Llama-3 fine-tuned on French with Llama-3 fine-tuned on Arabic; (b) Amortized Pareto front on merging Llama-3 fine-tuned on Chinese with Llama-3 fine-tuned on Japanese. The yellow line represents the evaluation metric of the corresponding single task model.

Merging Language Models Specializing in Math and Code Following DARE ((Yu et al., 2023)), we also experimented with merging two language models each with 13B parameters specializing in mathematics (referred to as the math model) and coding (referred to as the code model). The base model used is Llama-2 13B[7], the math model is WizardMath-13B[8], and the code model is llama-2-13b-code-alpaca[9]. Both the math and code models are fine-tuned versions of Llama-2 13B.

The primary reason for selecting Llama-2 as the base model, rather than newer models like Llama-3 or Qwen-2.5, is the lack of suitable math and code models fine-tuned from the same base configuration. For instance, although Qwen-2.5 provides both Qwen-2.5-Math and Qwen-2.5-Coder, the two models differ significantly in their configurations, specifically, the rope theta parameter is set to 10,000.0 for the math model and 1,000,000.0 for the coder model. This discrepancy makes it challenging to effectively merge these models. Please refer to Figure 9 for a visualization of the Pareto front obtained from MAP and Table 7 for GD and IGD metrics between the Pareto fronts obtained from Grid Search and from MAP.

Table 7: The GD and IGD metrics score for Arabic+French, Chinese+Japanese and Math+Code between the Pareto fronts find by Grid Search and find by MAP.

	GD	IGD	GD+IGD
Arabic+French	$0.023_{0.010}$	$0.035_{0.018}$	$0.058_{0.028}$
Chinese+Japanese	$0.014_{0.013}$	$0.028_{0.017}$	$0.041_{0.026}$
Math+Code	$0.039_{0.009}$	$0.0.018_{0.002}$	$0.057_{0.008}$

[7] https://huggingface.co/meta-llama/Llama-2-13b-hf

[8] https://huggingface.co/vanillaOVO/WizardMath-13B-V1.0

[9] https://huggingface.co/layoric/llama-2-13b-code-alpaca

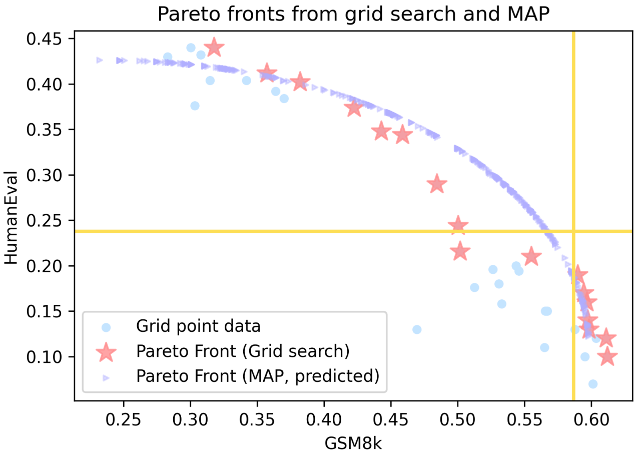

Figure 9: Amortized Pareto front by MAP on merging WizardMath-13B and code-alpaca-13B. The yellow line represents the evaluation metric of the corresponding single task model.

D.5 Additional experiment results on ResNet

We performed additional experiments on ResNet18 (He et al., 2016) by merging two models finetuned on CIFAR10 (Krizhevsky et al., 2009) and Flowers102 (Nilsback & Zisserman, 2008) and show the obtained Pareto front in Figure 10. Unlike ViT models, which perform zero-shot classification, ResNet requires additional fine-tuning of the classification head after model merging. We demonstrate that our method still applies to those models.

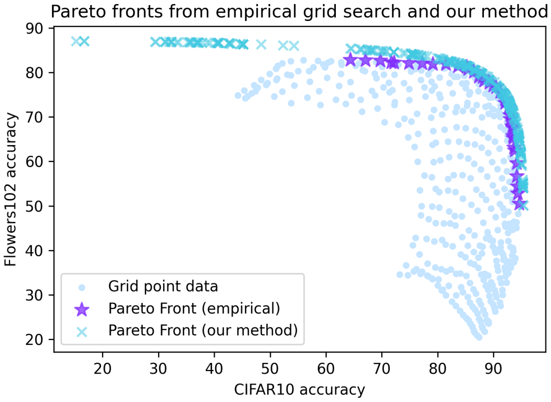

Figure 10: Pareto front obtained for two ResNet18 models on CIFAR-10 and Flowers-102. We perform additional finetuning of the classification head after merging the model weights.

E More Details on Algorithms

E.1 Plain MAP

It is important to note that Plain MAP (Algorithm 1) is an out-of-the-box plugin-like method. Many parts of it are kept generic: there are multiple ways to sample Ω in terms of the number of $\mathbf{c}$ and the style of sampling (Bayesian or not), thus creating a tradeoff between the quality of the Pareto front and the computational time; the task vector can be computed on the more memory-capable CPU and possibly in a parameter-efficient manner (e.g. LoRA, Adapter, and BiTFiT): for example, computing $\mathbf{v}_n$ via the subtraction of two full 7B models requires $2 \times 23 = 46$GB of memory capacity, but the memory cost for PEFT models may reduce to 16MB by only subtracting the non-frozen components; the for-loops in lines 2 and 4 can be computed in parallel, possibly using a much smaller subset of the data, and thus enjoying a computational speed-up.

E.2 Nested-Merging MAP

E.2.1 Overview

In this section, we explain the procedure of the algorithm in Figure 4 in detail.

Empirically, we only need 20 scaling coefficients to get a Pareto front of good quality to merge 2 tasks. However, due to the curse of dimensionality, we need exponentially more pairs of $(\mathbf{c}, \{\tilde{M}_n(\theta_m(\mathbf{c}))\}_{n=1}^N)$ pairs to achieve a good quality of the Pareto front in the case of 8 tasks. Theoretically, in the best case, the number of points required to obtain a good quality Pareto front for N tasks is $O(N^3)$. In the worst case, when the curse of dimensionality dominates, it could be $O(N \cdot 2^N)$. Using the nested merging scheme, we reduce the computation complexity from $O(N \cdot 2^N)$ to $O(N \log N)$. Please refer to Table 8 for the detailed computational complexity comparison. Algorithm details are presented in Algorithm 2.

Algorithm 2 Nested-merging MAP

```
Input: A predetermined preference pref $\in \mathbb{R}^N$ over the $N$ tasks, the tuple of task, loss, task vector:
       $G_n = (\text{task}_n, l_n, \boldsymbol{\theta}_{ft}^n)$
Normalize pref to make sure the sum is 1
Initialize the set $\tau = \{G_1, \ldots, G_N\}$
while $|\tau| > 1$ do
    Find the pair of $(G_i, G_j) \in \tau$ that are closest to each other in terms of $(l_i, l_j)$
    Implement Algorithm 1 to find the Pareto front $\text{PF}_{i,j}$ between $(\tilde{M}_i, \tilde{M}_j)$
    Select $\mathbf{c}^* = (c_i^*, c_j^*) \in \mathbb{R}^2$ based on the Pareto front $\text{PF}_{i,j}$
    Merge the models by $\boldsymbol{\theta}_{\text{merge}}^{i,j} = \boldsymbol{\theta}_{\text{pre}} + c_i(\boldsymbol{\theta}_{\text{pre}} - \boldsymbol{\theta}_{ft}^i) + c_j(\boldsymbol{\theta}_{\text{pre}} - \boldsymbol{\theta}_{ft}^j)$
    Calculate the weighted average loss on the two tasks $l_{ij} = \mathit{pref}_i l_i + \mathit{pref}_j l_j$
    Update $\tau$ by replacing $\{G_i, G_j\}$ with $\{G_{ij}\}$, where $G_{ij} \equiv (\text{task}_{i,j}, l_{ij}, \boldsymbol{\theta}_{\text{merge}}^{i,j})$
end
return $\boldsymbol{\theta}_{merge}^{1,2,\ldots,N}$
```

E.2.2 Time Complexity of Nested-Merging MAP

Table 8: Computational cost of MAP variants for N models.

	# evals per task	minimum # evals (total)	# evals (total)
Plain MAP	$O(N^2)$	$O(N^3)$	$O(N \cdot 2^N)$
Nested-merging MAP	$O(1)$	$O(N \log N)$	$O(N \log N)$

To estimate the computational complexity of nested-merging MAP, we denote N as the number of tasks. The number of total evaluations needed for nested-merging MAP is: $N/2 \times 2 + \ldots + N/2^m \times 2^m = O(N \log N)$ where $2^{m-1} < N \leq 2^m$.

Detailed calculations are as follows. When the number of tasks is 8, in the first rounds, four 2-task merging procedures are running in parallel. Each of the procedures evaluates 2 tasks. In the procedure of model-merging between 2 tasks, as discussed, we need to sample 20 scaling coefficients $\mathbf{c}$ and evaluate 20 merged models on the 2 tasks. Thus, it takes $4 \times 20 \times 2 = 160$ times of evaluation in the first round. In the second round, 2 2-task merging procedures are running in parallel, each of them evaluating 4 tasks. Thus, it takes $2 \times 20 \times 4 = 160$ times of evaluation. In the last round, there is only one 2-task merging and evaluation on 8 tasks. It takes $1 \times 20 \times 8 = 160$ times of evaluation. In total, NMMAP takes 480 times of evaluations. Generalizing the calculation, the number of rounds can be calculated by $\log N$. In each round, we need to evaluate $T \cdot N/2^i \cdot 2^i = TN$ where T is the number of scaling coefficient vectors needed to be evaluated when the number of tasks is 2. In the above example, $T = 20$. Thus, the time complexity is $O(TN \log N)$. We rewrite it as $O(N \log N)$ if ignoring T which is a constant.

E.2.3 Explanation of curse of dimensionality

Figure 11 illustrates the curse of dimensionality through the discretizations of scaling coefficients for task-specific optimization. The left plot shows a 2D grid of scaling coefficients for two tasks, while the right plot extends this to three tasks (i.e., a 3D grid). In both cases, the space of possible scaling coefficients is discretized uniformly, with a resolution determined by the parameter `pts_per_dim`, which refers to the number of discretized points along each axis (dimension). The spacing between adjacent points, denoted as Δ, is given by $\Delta = \frac{1}{\texttt{pts\_per\_dim}-1}$. As the number of dimensions (tasks) increases, the total number of grid points grows exponentially. Specifically, the number of grid points in d dimensions is given by $(\texttt{pts\_per\_dim})^d$, leading to a combinatorial explosion in the search space. This exponential growth exemplifies the *curse of dimensionality*, rendering brute-force search methods computationally infeasible as the number of tasks (dimensions) increases beyond a small threshold. Therefore, while grid search may be adequate for low-dimensional problems, it quickly becomes impractical in higher-dimensional settings.

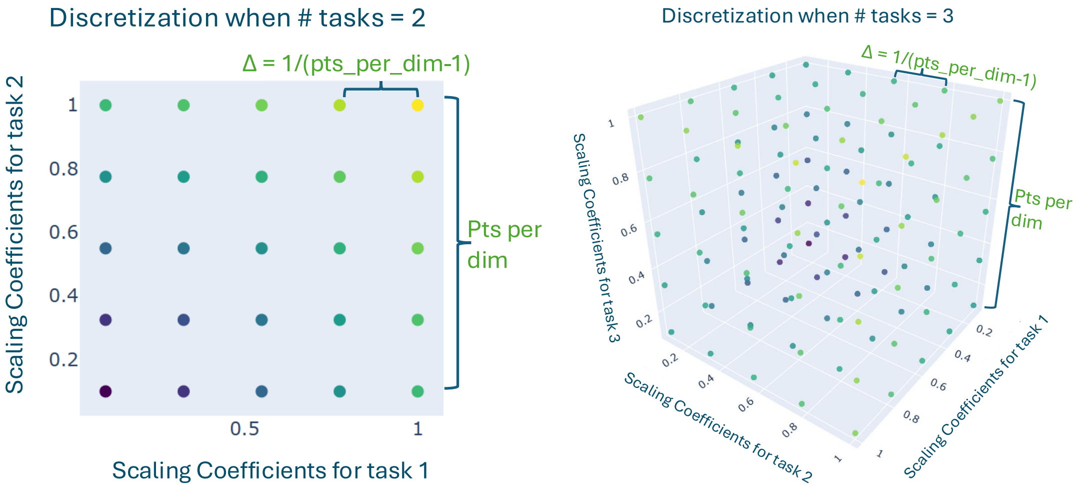

Figure 11: The discretization of scaling coefficients when the number of tasks is 2 and 3. As the dimension grows, preserving the same number of pts per dimension results in exponentially more grid points. This serves to illustrate why when the dimension is low (e.g., < 4), we can regard the brute-force direct search method as ground truth, but it becomes insufficient when the dimension is higher.

E.2.4 Intermediate Pareto Fronts in Each Round

To determine if NMMAP affects performance negatively when compared to merging multiple models in a single operation. We show the intermediate Pareto fronts obtained when merging 8 models using nested-merging MAP in Figure 12, where we merge two models at a time. The figures illustrate the intermediate Pareto fronts obtained, where A_B means the model obtained by merging model A and model B.

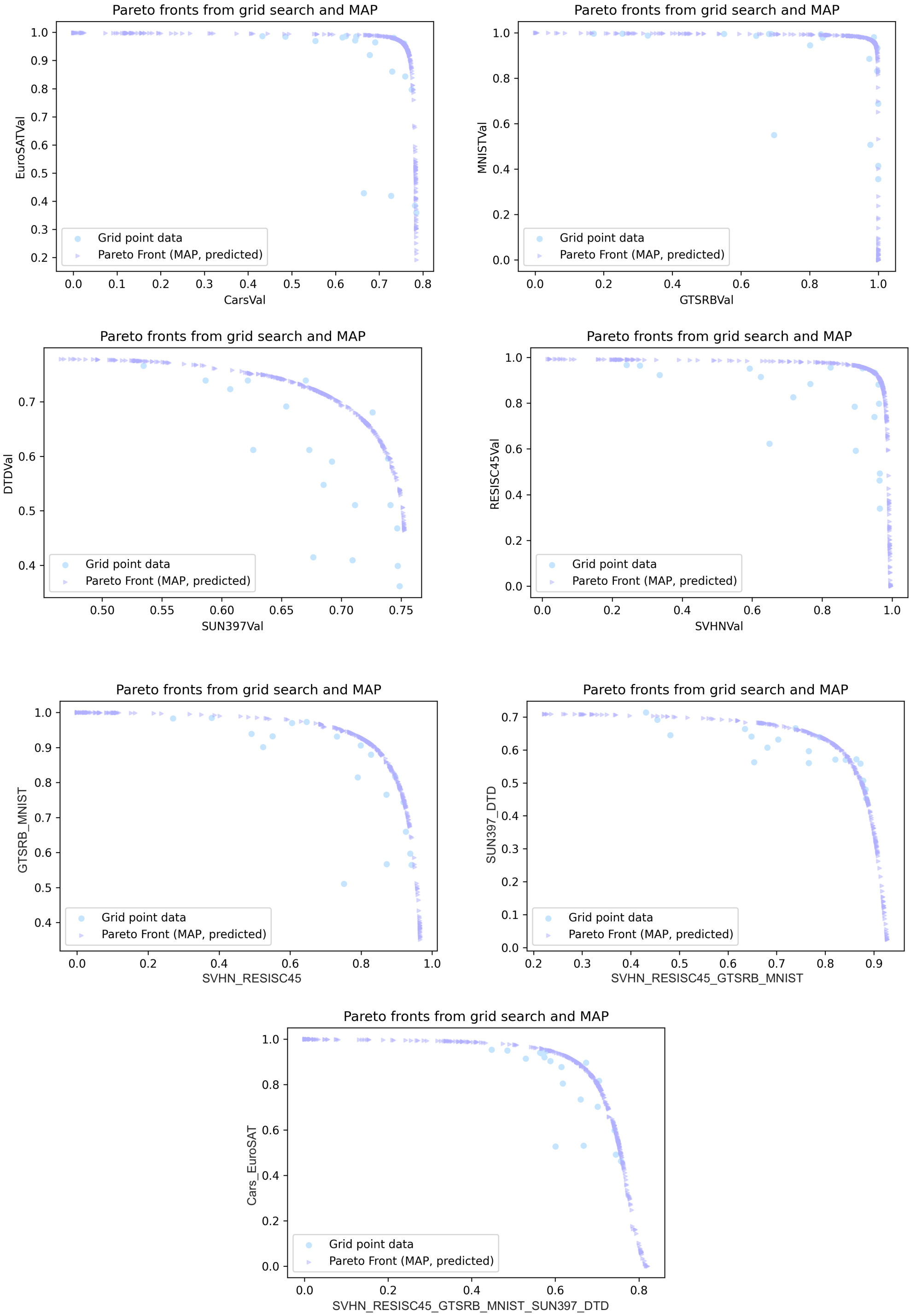

Figure 12: Illustration of the sequential steps involved in merging 8 models using nested-merging MAP (left to right, top to bottom). The figures show the intermediate Pareto fronts obtained, where A_B means the model obtained by merging model A and model B.

E.2.5 Results on using nested merging to merge 8 models

We further evaluate the effectiveness of nested-merging MAP. Supplemental Figure 12 shows the intermediate Pareto fronts obtained using nested-merging MAP (NMMAP) sequentially. In addition, we compared the performance of NMMAP with Plain MAP (Algorithm 1). The results are shown in Table 9. The results confirm that nested-merging MAP can obtain comparable results to those obtained by MAP while using much fewer evaluation runs. As discussed in Appendix E.2.2, in total, we run $40 \times 4 + 80 \times 2 + 160 \times 1 = 480$ evaluations. In contrast, when running the Plain MAP (Algorithm 1), we used 280 coefficients and evaluate $280 \times 8 = 2240$ times. In addition, while being suboptimal to MAP (Algorithm 1), nested-merging MAP can still outperform other baseline methods such as TA and DARE-TA in accommodating various user preferences with relatively low computational cost, especially when the number of tasks is high.

Table 9: We compared nested-merging MAP with MAP and baseline methods in merging 8 models using a set of 10 preference vectors in terms of preference-weighted sum of accuracies.

Metric	Single-task models	Nested-merging MAP	Plain MAP	TIES-merging	DARE-TIES	Task Arithmetic (TA)	DARE-TA
Preference weighted sum (↑)	90.05±3.02	67.05±3.89	**72.12**±3.78	70.79±3.81	70.51±3.58	59.44±5.68	63.14±4.91

E.3 Bayesian MAP

We further improve the efficiency of MAP by proposing an adaptive Bayesian sampling algorithm. This Bayesian approach samples the points from regions with the highest level of uncertainty, where uncertainty is quantified with the Upper Confidence Bound (UCB). Please refer to Algorithm 3 for more details about the algorithm.

The discretization method shown in the Figure 13 illustrates how continuous decision variables $\mathbf{c}$ are divided (or "binned") based on their angular components, in either 2D polar or 3D spherical coordinate systems.

In general, a point $\mathbf{c} = (c_1, c_2, \ldots, c_n)$ in spherical coordinates is represented using:

$$\begin{cases} c_1 = r \cos \phi_1 \\ c_2 = r \sin \phi_1 \cos \phi_2 \\ c_3 = r \sin \phi_1 \sin \phi_2 \cos \phi_3 \\ \vdots \\ c_{n-1} = r \sin \phi_1 \cdots \sin \phi_{n-2} \cos \phi_{n-1} \\ c_n = r \sin \phi_1 \cdots \sin \phi_{n-2} \sin \phi_{n-1} \end{cases}$$

where $r = \|\mathbf{c}\|_2$ is the radial distance (magnitude), $\phi_1, \ldots, \phi_{n-2} \in [0, \pi]$, $\phi_{n-1} \in [0, 2\pi]$.

To discretize the **direction** (angular component) of a decision vector $\mathbf{c} \in \mathbb{R}^n$, we follow the steps below:

1. **Normalization:** Convert $\mathbf{c}$ to a unit vector:

$$\hat{\mathbf{c}} = \frac{\mathbf{c}}{\|\mathbf{c}\|_2}$$

2. **Conversion to Spherical Coordinates:** Represent the direction of $\mathbf{c}$ using $(n-1)$ spherical angles $(\phi_1, \phi_2, \dots, \phi_{n-1})$. These can be computed recursively as follows:

$$\begin{aligned}
\phi_1 &= \arccos\left(\frac{c_1}{\sqrt{c_1^2 + c_2^2 + \cdots + c_n^2}}\right) \\
\phi_2 &= \arccos\left(\frac{c_2}{\sqrt{c_2^2 + \cdots + c_n^2}} \Bigg/ \sin\phi_1\right) \\
&\vdots \\
\phi_{n-2} &= \arccos\left(\frac{c_{n-2}}{\sqrt{c_{n-2}^2 + c_{n-1}^2 + c_n^2}} \Bigg/ \prod_{j=1}^{n-3} \sin\phi_j\right) \\
\phi_{n-1} &= \arctan\left(\frac{c_n}{c_{n-1}}\right)
\end{aligned}$$

3. **Discretization of Angular Space:** Divide each angle ϕ_i into k_i uniform bins. For example, if $k_i = 4$, then:

$$\phi_i \in \left[\frac{j\pi}{2k_i}, \frac{(j+1)\pi}{2k_i}\right), \quad \text{for } j = 0, 1, \dots, k_i - 1$$

where the angular domain is restricted to $[0, \pi/2]$ to ensure non-negativity in all coordinates.

4. **Bin Assignment:** The final bin index for $\mathbf{c}$ is a tuple of angular bin indices:

$$\text{bin}(\mathbf{c}) = (b_1, b_2, \dots, b_{n-1}), \quad \text{where } b_i = \left\lfloor \frac{\phi_i}{\Delta\phi_i} \right\rfloor$$

and $\Delta\phi_i = \frac{\pi}{2k_i}$ denotes the bin width for ϕ_i.

Each bin corresponds to a distinct angular sector, grouping together direction vectors with similar orientations, regardless of their magnitudes.

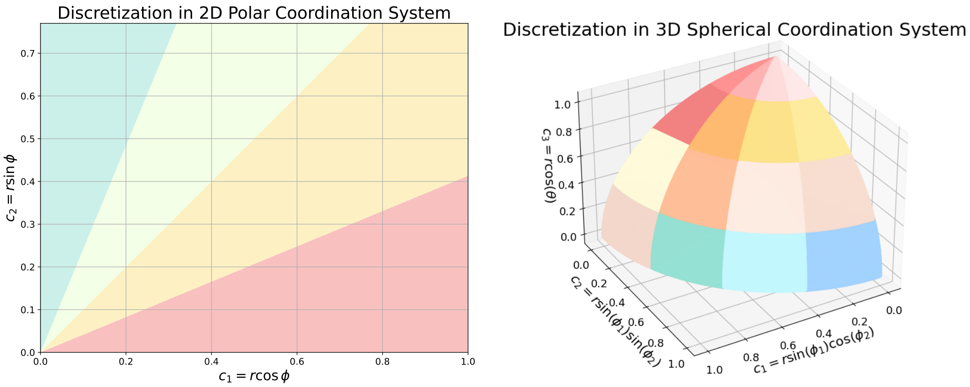

(a)

(b)

Figure 13: (a) Discretizing of two task scaling coefficients along the angular dimension in 2D polar coordinate system; (b) Discretizing of three task scaling coefficients along the angular dimensions in 3D spherical coordinate system.

Algorithm 3 Bayesian Adaptive of Surrogate Model

```
Input: Number of iterations $J$, Buffer $\mathcal{B}$, Pretrained model $\boldsymbol{\theta}_{\text{pre}}$, Task vectors $\mathbf{v}_n$, Evaluators for
    task $N$, $M_n(\cdot)$, Discretization bin number $K$, sample size for every iteration $n_j$, $j = 0$ to $J$,
    Bootstrap dropping rate $\alpha = 20\%$, Bootstrap sampling number $Q = 30$.
$\mathcal{B} \leftarrow \emptyset$
for $j = 0$ to $J$ do
    if $j = 0$ then
        Sample $n_0$ scaling coefficients $\{\mathbf{c}_i\}_{i=1}^{n_j}$ from $U([0,1]^N)$
    else
        Sample $n_j$ scaling coefficients $\{\mathbf{c}_i\}_{i=1}^{n_j}$ based on the posterior distribution
    end
    for $i = 0$ to $n_j$ do
        Merge the model $\theta_m(\mathbf{c}_i) = \boldsymbol{\theta}_{\text{pre}} + \mathbf{c}_i \cdot \mathbf{v}_n$ Evaluate $m_{n,i} = M_n(\theta_m(\mathbf{c}_i))$ $\mathcal{B} \leftarrow \mathcal{B} \cup \{(\mathbf{c}_i, m_{n,i})\}$
    end
    Fit the quadratic approximation surrogate model $\tilde{M}_n$ by learning $\mathbf{A}_n^*, \mathbf{b}_n^*, e_n^*$ in Equation (5).
    Discretize the scaling coefficients along the angular dimensions in hyper-spherical coordinates
      (see Figure 13 as examples)
    for $k = 0$ to $K$ do
        Calculate the mean of $L2$ loss between $\tilde{M}_n(\mathbf{c}_i)$ and $M_t(\mathbf{c}_i)$, where $\mathbf{c}_i$ are in bin $k$, denoted
          as mean$_k$
        Bootstrap to estimate the standard deviation of the losses.
        for $q = 0$ to $Q$ do
            Randomly (uniformly) drop $\alpha$ scaling coefficient in bin $k$ Calculate the mean of $L2$ loss
              between $\tilde{M}_n(\mathbf{c}_i)$ and $M_t(\mathbf{c}_i)$ with the rest points and denoted with $l_q$
        end
        Calculate the standard deviation of the $\{l_q\}_{q=0}^{Q}$ and denoted as std$_k$ score$_k$ = mean$_k + \frac{1}{2}$std$_k$
    end
    Calculate probability distribution across the discretized bins by score$_k$ as the posterior sampling
      strategy in the next round
end
```

E.3.1 Performance of Bayesian MAP

Please refer to Figure 14 for the experimental results comparing Bayesian MAP Algorithm 3 with MAP Algorithm 1. The very left column shows the names of the 2 tasks being merged. Below, we define points (pts) as scaling coefficients and evaluation metrics of the corresponding merged models. Please note that the results shown in this figure are the mean of 7 merging tasks that merge 2 models: DTD+Cars, DTD+RESISC45, EuroSAT+RESISC45, GTSRB+Cars, GTSRB+RESISC45, RESISC45+SVHN, SUN397+SVHN. The Pareto front estimated by Bayesian MAP with only one iteration (6+3 pts) is shown in Figure 15.

The experiments are initialized with 6 pairs of $\mathbf{c}$, $\{M_n\}_{n=1}^N$ (iter 0). In every following iteration, we sample more points following the Bayesian adaptive sampling algorithm. We compare the Bayesian adaptive sampling beginning with 6 points and adding 3 additional points ($6 + 3$ pts) with running Algorithm 1 with 9 points in a row. We also compare the Bayesian adaptive sampling beginning with 6 points and adding 3 additional points for 2 times ($6 + 2 \times 3$ pts) with running Algorithm 1 with 12 points in a row. We show that, in most cases, utilizing the same number of points, Bayesian adaptive sampling performs better than the run-in-a-row scheme in Algorithm 1.

In conclusion, when the number of data points (scaling coefficients and evaluation metrics of the corresponding merged models) is small, Bayesian MAP Algorithm 3 performs better than MAP Algorithm 1. As the number of data points increases, their performance becomes closer. Thus, we recommend implementing Bayesian MAP when computational resources are very limited and the number of models (tasks) to merge is not high.

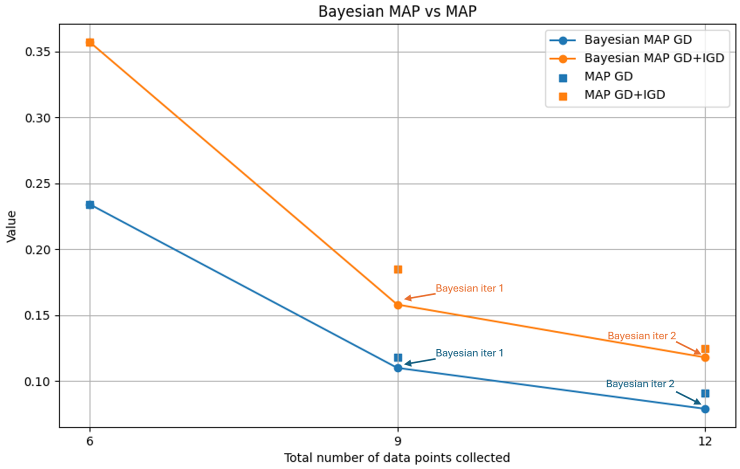

Figure 14: Bayesian MAP compared to MAP. The x-axis represents the number of points used by either MAP or Bayesian MAP, while the y-axis represents the value for IGD or GD. We compared MAP with 6, 9, and 12 points, and Bayesian MAP with 6 initial points, sampling 3 more points each round for two rounds.

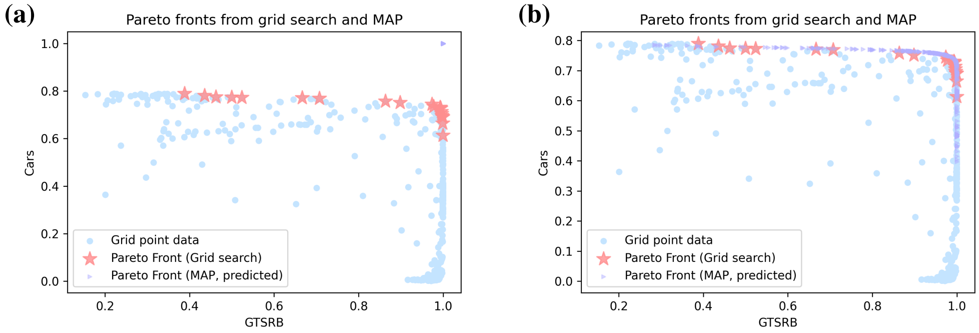

Figure 15: (a) This plot shows a failure case of the amortized Pareto front when we only have 6 initial randomly sampled pairs of $(\mathbf{c}, \{M_i(\theta_m(\mathbf{c}))\}_{i=1}^N)$ (b) After one iteration of Bayesian adaptive sampling for 3 more pairs (9 in total), the amortized Pareto front is much better than the initial Pareto front.

F Potential Q & A

In this section, we anticipate and address some potential questions that readers might have.

F.1 The authors assume a setting where it is computationally expensive to query the model evaluations. But is this the reality?

Yes, to get the Pareto front of tasks that have trade-offs. We need to have a lot of data points to show the trade-off. Here, each data point is the evaluation metric of a model. To get the ground truth evaluation metric of a task (e.g. let's say classification), we need to run the evaluation script of the model to determine the metric. If we have 4 tasks, and we set 5 possible values (let's say 0.2, 0.4, 0.6, 0.8, 1) for the scaling coefficient vector of each model specialized for one task. We will have to evaluate $5^4 = 625$ models on all 4 tasks. Assuming each evaluation takes 1 minute, evaluating all the models on all the 4 tasks will take 625 models $\times$ 4 tasks $\times$ 1 minute $= 2500$ minutes $= 41.7$ hours which is expensive. In big O notation, assuming we have T tasks, the time of evaluation for each task is T. The time (computational) complexity is $O(TN2^N)$.

F.2 How is MAP different from other MOOP methods, such as linear scalarization?

Computational Efficiency MAP is computationally efficient because it leverages a surrogate model (the quadratic approximation) to estimate the evaluation metrics for different model combinations. Once the quadratic model is learned, solving the optimization problem (approximating the Pareto front) is much faster because the complexity is reduced to optimizing over the quadratic approximation, rather than needing to directly evaluate the task metrics over the entire solution space.

Additionally, MAP does not require gradient descent or re-training when merging models and the surrogate model provides an efficient way to approximate the Pareto front without re-evaluating every model configuration.

On the other hand, linear scalarization involves computing a weighted sum of the objectives and solving it as a single-objective optimization problem. However, it often requires multiple optimization runs with different weight configurations to explore different points on the Pareto front. Since linear scalarization does not model non-linear relationships, it might require more iterations or grid searches over different weights to achieve a decent approximation of the Pareto front. This can become computationally expensive, especially for a large number of tasks or highly complex models.

Non-convex Pareto Fronts Many real-world multi-objective optimization problems have nonconvex Pareto fronts, which require more sophisticated methods. While linear scalarization can only explore the convex regions of the Pareto front, NSGA-III allows MAP to discover nonconvex regions of the Pareto front. It does this by evolving a population of solutions that are non-dominated (i.e., not Pareto dominated by any other solution) and spreading these solutions across the entire Pareto front, including both convex and non-convex regions.

F.3 Why does quadratic approximation have a lower cost?

For the MAP algorithm (Algorithm 1), the time complexity is the same as what we mentioned above; what is different is that we fitted an approximation of the evaluation metrics. We only need the scaling coefficient vectors to input to a quadratic function model to be able to get the estimated evaluation score. Running the quadratic function once takes only $3.91 \times 10^{-6}s \pm 894 \times 10^{-9}s$. Thus, evaluating 2500 times takes $< 2500 \times 4 \times 10^{-6}s = 10^{-2}s$.

F.4 Why not compare to Git-Rebasin (Ainsworth et al., 2023)?

We did not compare our method to Git Re-Basin because their study focuses on the scenarios of merging the models from different initializations, whereas our background works on the same initialization of different fine-tuned models.

F.5 Why does nested-merging MAP not give a complete Pareto front?

In nested-merging MAP, we merge the models in pairs. For example, there are $model_i$ for task i as individual fine-tuned models where $i = 1, 2, 3, 4$. We first merge model 1 and model 2 given the preference of the user between task 1 and task 2. We then get $model_{1,2}$. At the same time, we merge model 3 and model 4 given the preference of the user between task 3 and task 4 and get $model_{3,4}$. Finally, we merge the $model_{1,2}$ and $model_{3,4}$ given the preference of user to get $model_{1,2,3,4}$. We output the $model_{1,2,3,4}$ as the output merged model of the algorithm. Please note that the merging order in the algorithm should be decided by the loss function clustering. It is a heuristic decision and does not always dominate other merging orders. Thus, we choose not to emphasize the contribution of this order. The practitioner may use any order they think can be helpful for merging.

F.6 It seems nested-merging MAP performs worse than MAP. What is the meaning of it?

In theory, the surrogate model can be easily fitted when the number of tasks is low. When it is high (e.g. 8), the fit of the surrogate model can no longer be a near-perfect approximation (please find the R^2 in Table 3). Thus, even if the NMMAP can only find the suboptimal solution, it is still comparable to MAP Algorithm 1 according to Table 9. We understand in general that NMMAP does not find the global optimum, but please kindly keep in mind that even if their performance is comparable, NMMAP takes way less computation for evaluation.

F.7 Why does nested-merging MAP not output the optimal solution?

The solution found by nested-merging MAP (NMMAP) is indeed suboptimal given the limited search space compared with merging all models at once. However, it does not mean that it is not useful in all situations. When the number of tasks is high, it has comparable performance to MAP while consuming much fewer computations for evaluation.

F.8 How do you deal with gradient and Hessian in the second-order Taylor expansion?

Notations:

- p as the number of parameters in the pre-trained model (also the number of parameters in each task vector).
- $\mathbf{V}$ is the matrix of task vectors of different N tasks. Thus, $\mathbf{V} \in \mathbb{R}^{p\times N}$.
- $\mathbf{c}$ is the scaling coefficient vector $\in \mathbb{R}^N$.
- M_n is the metric (e.g. accuracy) for the task n.

$$\begin{aligned} M_n(\mathbf{c}) &= \underbrace{M_n(\boldsymbol{\theta}_{\text{pre}})}_{\in\mathbb{R}} + \underbrace{\nabla M_n(\boldsymbol{\theta}_{\text{pre}})^\top}_{\in\mathbb{R}^{1\times p}} \underbrace{\mathbf{V}}_{\in\mathbb{R}^{p\times N}} \underbrace{\mathbf{c}}_{\in\mathbb{R}^{N\times 1}} + \frac{1}{2} \underbrace{(\mathbf{V}\mathbf{c})^\top}_{\in\mathbb{R}^{1\times p}} \underbrace{\mathbf{H}_n(\boldsymbol{\theta}_{\text{pre}})}_{\in\mathbb{R}^{p\times p}} \underbrace{\mathbf{V}\mathbf{c}}_{\in\mathbb{R}^{p\times 1}} + \underbrace{R_n}_{\in\mathbb{R}} && (6) \\ &= \underbrace{e_n}_{\in\mathbb{R}} + \underbrace{\mathbf{b}_n^\top}_{\in\mathbb{R}^{1\times N}} \underbrace{\mathbf{c}}_{\in\mathbb{R}^{N\times 1}} + \underbrace{\mathbf{c}^\top}_{\in\mathbb{R}^{1\times N}} \underbrace{\mathbf{A}_n}_{\in\mathbb{R}^{N\times N}} \underbrace{\mathbf{c}}_{\in\mathbb{R}^{N\times 1}} && (7) \\ & && (8) \end{aligned}$$

$$\tilde{M}_n(\mathbf{c}; \mathbf{A}_n, \mathbf{b}_n, e_n) \equiv e_n + \mathbf{b}_n^\top \mathbf{c} + \frac{1}{2}\mathbf{c}^\top \mathbf{A}_n \mathbf{c}$$

where

$$\mathbf{A}_n = \mathbf{V}^\top \mathbf{H}_n(\boldsymbol{\theta}_{\text{pre}})\mathbf{V} \in \mathbb{R}^{N\times N}, \mathbf{b}_n = \mathbf{V}^\top \nabla M_n(\boldsymbol{\theta}_{\text{pre}}) \in \mathbb{R}^N, e_n = M_n(\boldsymbol{\theta}_{\text{pre}}) + R_n \tag{9}$$

Please notice that $\mathbf{A}$ is a symmetric matrix. Specifically, when the number of tasks is 2, we have:

$$\begin{aligned}
\tilde{M}_1(\mathbf{c}; \mathbf{A}_1, \mathbf{b}_1, e_1) &\equiv e_1 + \mathbf{b}_1^\top \mathbf{c} + \frac{1}{2}\mathbf{c}^\top \mathbf{A}_1 \mathbf{c} && (10)\\
&= \frac{1}{2}A_{1,11}c_1^2 + A_{1,12}c_1c_2 + \frac{1}{2}A_{1,22}c_2^2 + b_{1,1}c_1 + b_{1,2}c_2 + e_1 && (11)\\
\tilde{M}_2(\mathbf{c}; \mathbf{A}_2, \mathbf{b}_2, e_2) &\equiv e_2 + \mathbf{b}_2^\top \mathbf{c} + \frac{1}{2}\mathbf{c}^\top \mathbf{A}_2 \mathbf{c} && (12)\\
&= \frac{1}{2}A_{2,11}c_1^2 + A_{2,12}c_1c_2 + \frac{1}{2}A_{2,22}c_2^2 + b_{2,1}c_1 + b_{2,2}c_2 + e_2 && (13)\\
& && (14)
\end{aligned}$$

We don't calculate the gradient or Hessian to get $\mathbf{A}_1$, $\mathbf{A}_2$, $\mathbf{b}_1$, $\mathbf{b}_2$, e_1 and e_2. We use linear regression to estimate them. How? Given a (c_1, c_2) pair, we can define a merged model $\boldsymbol{\theta}_{\text{merge}}(c_1, c_2)$. We evaluate the merged model on task 1 and task 2 to get the metrics (e.g. accuracy). Given 20 pairs of (c_1, c_2), we would be able to evaluate and get 20 corresponding, (M_1, M_2) which are metrics for task 1 and task 2. Thus, we can fit the surrogate model $\tilde{M}_1(\mathbf{c}; \mathbf{A}_1, \mathbf{b}_1, e_1)$ and $\tilde{M}_2(\mathbf{c}; \mathbf{A}_2, \mathbf{b}_2, e_2)$.